ABSTRACT

Title of Thesis:
Photogrammetric Reconstruction of
Tandem-Wing Kinematics for Free-Flying
Dragonflies Undergoing a Range of
Flight Maneuvers

Mateusz J. Gabryszuk, Master of Science, 2017

Thesis directed by:
Professor Stuart Laurence
Department of Aerospace Engineering

Photogrammetric methods are used to reconstruct the body and wing kinematics of free-flying dragonflies. A novel experimental setup was designed and constructed to allow for repeated untethered flights in a constrained flight arena. Kinematic data are presented for twelve individual flights and a total of 23 complete wing strokes, including unaccelerating, accelerating, climbing, and turning flight. High variability is observed in the wing motions employed by individual dragonflies, particularly in terms of stroke amplitude, pitch angle, and wingbeat frequency. Forewing and hindwing flapping is found to be neither in phase nor fully out of phase across all cases, with the forewings lagging the hindwings by an average of 90 degrees. Downstroke durations are observed to be shorter than upstroke durations except in highly accelerating flights. Migratory dragonflies are found to exhibit notably different wing kinematics than non-migratory species.

Photogrammetric Reconstruction of Tandem-Wing Kinemacts for
Free-Flying Dragonflies Undergoing a Range of Flight Maneuvers

by

Mateusz Jerzy Gabryszuk

Thesis submitted to the Faculty of the Graduate School of the
University of Maryland, College Park in partial fulfillment
of the requirements for the degree of
Master of Science
2017

Advisory Committee:
Professor Stuart Laurence, Chair/Advisor
Professor Inderjit Chopra
Professor Imraan Faruque

Acknowledgments

This thesis, and all the accomplishments that came before it, would not have been possible without the support and guidance of my parents. Raised by two scientists, I was constantly pushed to leave my comfort zone and seek out new challenges. They deserve credit for all of my successes, and this thesis is no exception.

I would like to thank my adviser, Dr. Stuart Laurence, for providing constant support and encouragement during the two years I spent on this work. Although his preferred research area was far away from the world of insect flight, he exhibited great interest and enthusiasm for this project, and was always able to guide me in the right direction. I would also like to thank the members of my committee, Dr. Inderjit Chopra and Dr. Imraan Faruque, for reviewing this work and providing insightful commentary.

I am further grateful to Dr. Faruque for allowing the use of his laboratory space for the purposes of this project. Gratitude is also extended to Dr. Sean Humbert and Dr. Anya Jones for the use of their high-speed cameras. I would also like to thank the U.S. Army Research Laboratory for providing funding to support this research.

A great deal of thanks is owed to Nathan Shumway, my partner on this monumental project. I sincerely appreciate the constant guidance that he was able to give me as I settled into the role of a graduate student. I would be remiss if I did not thank him for the countless hours he spent helping me extract marker data from test images, a process that I am sure we both will not miss in years to come.

Finally, I owe a debt of gratitude to my incredibly supportive girlfriend Jordan, who always helps me stay positive no matter how overwhelmed I may feel.

Table of Contents

List of Tables

List of Figures

Chapter 1:   Background and Motivation

1.1   Micro Air Vehicles

Recent advancements in processor power, energy storage, automation, and sensing have stimulated interest in the development of small-scale aerial platforms. Particular focus has been placed on micro air vehicles (MAVs), a class of unmanned aerial vehicle (UAV) generally defined as having a maximum dimension of less than 15 cm. Development work has been led primarily by the United States Department of Defense, with the goal of designing a low-cost, small-scale reconnaissance vehicle that can operate within confined areas such as buildings or tunnels. A general set of MAV design requirements is shown in Table 1.1.

The area of MAV design is still in its infancy due to the lack of established design tools for such small-scale flying vehicles and a general lack of understanding of the low Reynolds number flight regime. Table 1.2 illustrates the performance of several early MAV vehicles. Most designs have used fixed- or rotary-wing configurations, but flapping-wing platforms have seen steadily increasing interest at the MAV scale. Notable examples include the CalTech/Aerovironment Microbat, the first MAV to utilize flapping-wing propulsion [2], and the University of Toronto Mentor MAV, the first bio-inspired MAV capable of hovering flight [3].

1

Table 1.1: General design requirements for MAVs. Adapted from [1].

Specification	Requirements	Details
Size	<15.24 cm	Maximum dimension
Weight	100 g	Objective GTOW
Range	1 to 10 km	Operational range
Endurance	60 min	Loiter time on station
Altitude	<150 m	Operational ceiling
Speed	15 m/s	Maximum flight speed
Payload	20 g	Mission dependent
Cost	$150	Maximum cost

1.1.1 Comparison of MAV Platform Types

The increased interest in developing MAV platforms has highlighted the challenge of designing an aerodynamically functional aircraft at such a small scale. MAVs typically operate at a Reynolds number of 10^5 or below [4], an aerodynamic regime where the steady-state mechanisms that are utilized by large fixed-wing aircraft begin to lose effectiveness. Increased flow separation and earlier laminar to turbulent transition introduce additional drag over an airfoil and decrease overall performance. The decline in performance with decreasing Reynolds number for both smooth and rough airfoils is shown in Figure 1.1. Rotary- and especially flapping-wing aircraft are better suited to such small scales, as they utilize unsteady aerodynamic mechanisms that allow them to generate much higher lift forces at low

Table 1.2: Performance specifications of early MAV designs. Adapted from [1].

Vehicle properties	Black Widow	LUMAV	Microbat	MICOR
GTOW, g	80	440	10.5	103
Cruise speed, m/s	13.4	5	5	2
Wing loading, N/m^2	40.3	-	40	-
Disk loading, N/m^2	-	185	-	25
Wing span or rotor diameter, cm	15.24	15.24	15.24	15.24
Max L/D	6	N/A	N/A	5
Endurance, min	30	20	2.27	3
Hover endurance	N/A	N/A	N/A	3
Power source	Li-ion batteries	2-stroke IC engine	NiCad N-50 cells	Li-ion batteries
Energy density, W-h/kg	140	5500	100	150
Hover power, W	N/A	70	N/A	11
Hover FM	N/A	0.41	N/A	0.55
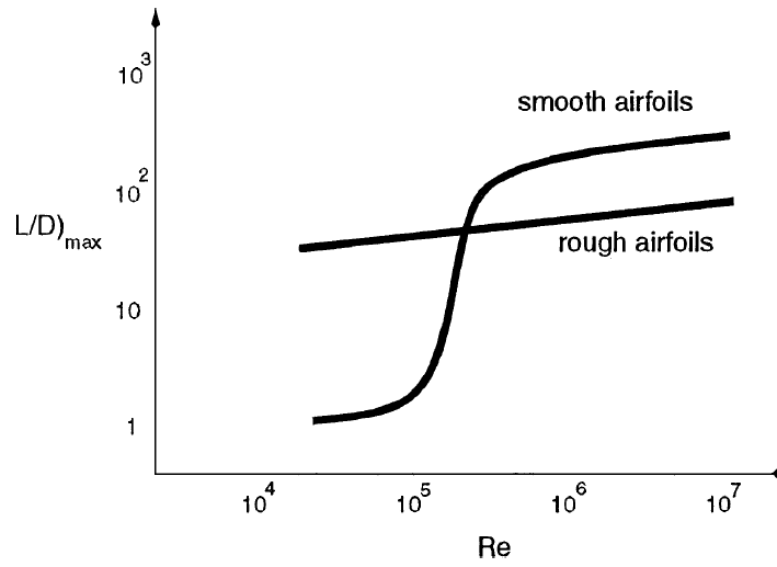
Figure 1.1: Aerodynamic performance of smooth and rough airfoils in the low Reynolds number regime. From [1].

Reynolds numbers than fixed-wing aircraft. Furthermore, fixed-wing aircraft are generally incapable of hovering or vertical takeoff and landing (VTOL), traits that are highly desirable for most MAV missions.

Rotary-wing platforms have seen great popularity at the MAV scale due to their maneuverability and ease of design. The long-time developmental history of manned rotorcraft has allowed for these concepts to be scaled down, preventing the need for a blank sheet design. Although the fundamental relationship between viscous and inertial fluid forces is inherently quite different at such small Reynolds numbers, the fundamental lift mechanisms used by rotorcraft remain the same at both scales.

Nevertheless, rotary-wing designs are not ideally suited to MAV scales for two primary reasons. First, a platform that was created and optimized for high Reynolds

4
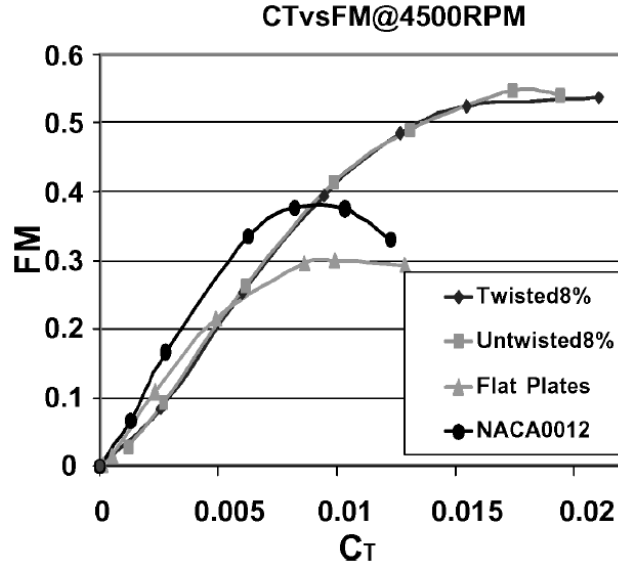
Figure 1.2: Figure of merit vs. thrust coefficient for MICOR MAV using various rotor airfoils. From [1].

number applications will inherently face aerodynamic limitations at radically lower Reynolds numbers. Rotary-wing MAVs suffer from poor efficiency, as shown in Figure 1.2. In this comparison of rotor airfoil geometries for the University of Maryland's MICOR MAV (see Table 1.2), the highest figure of merit achieved is approximately 0.55. By comparison, full-scale rotorcraft typically operate at a figure of merit between 0.65 and 0.85 [1]. The decrease in efficiency is primarily due to an increase in rotor profile losses; at low Reynolds numbers as much as 45 percent of the rotor power can be consumed by profile losses, as compared to 30 percent for full-scale aircraft. Rotorcraft are still useful at the high end of the MAV size scale but encounter design problems at very small scales due to limitations in aerodynamic efficiency, maneuverability, and energy storage.

1.2 Flying Insects

For the above-mentioned reasons, much attention has turned to flapping-wing flight mechanisms to propel small MAV designs. Nature has proven that this type of flight mechanism is effective at a range of Reynolds numbers from as low as 100 (for small insects such as fruit flies) to as high as 14,000 (for large insects and hummingbirds) [5]. Larger birds such as hawks and eagles can fly at higher Reynolds numbers, but frequently utilize gliding kinematics and are unable to hover. Difficulties with scaling down motors and batteries apply to flapping-wing aircraft as well, but they have the potential to require smaller hardware due to their higher aerodynamic efficiency. Flapping-wing designs are inherently more challenging to implement because of the lack of historical development in the area, but nature provides us with a wide range of species that can be studied to discover the secrets of low Reynolds number flight.

There exist nearly one million species of flying insects and over 10,000 flying vertebrates [4], representing an enormous number of variations on biological flight. Flying insects range in scale from *Drosophila*, tiny fruit flies operating at a Reynolds number of 100, to the *Ornithoptera alexandrae*, a giant butterfly with a wingspan of 25 cm. Some, such as honey bees, employ only one pair of wings, while others, such as damselflies, use a tandem set of wings. With so many candidates for study, it can be daunting to choose a particular species for detailed investigation. Nevertheless, it is apparent that certain insect types are more capable than others and thus serve as better archetypes for bio-inspired MAVs.

1.2.1 The Dragonfly as a Candidate for Study

Within the world of flying insects, dragonflies (order *Odonata*, infraorder *Anisoptera*) in particular are a primary candidate for kinematic and aerodynamic study. They are somewhat unique in their use of tandem wing pairs rather than a single set of flight wings. Odonata possess separate flight muscles for the forewing and hindwing, giving them fine control of each wing independent of the motion of the other three [6]. Dragonflies are capable of controlling the pitch, flap, and elevation angles of their wings, and can likely vary the phasing of changes in each of these parameters. This fine range of control allows dragonflies to be incredibly fast and maneuverable in the air; they are able to fly forwards and backwards or hover in place.

This speed and agility is vital to dragonflies' survival due to their ecological status as predators - a role they perform extremely well. Dragonflies prey exclusively on insects, including flies, mosquitoes, and even other dragonflies. Because their prey is highly maneuverable, dragonflies have evolved to become some of the highest performing fliers on the planet. Furthermore, dragonflies' high energy output requires them to spend a great deal of their day hunting. A study of *Pantala flavescens* in Japan estimated that members of the species needed to consume 14 mg of food each day, corresponding to 185 small insects [7]. They cannot afford to expend energy in frequent failed pursuits of prey, and they rarely do: studies have found that once a dragonfly initiates a pursuit of fruit fly prey, its success rate is 92-97 percent [8] [9]. This greatly exceeds the predatory success rate of other

apex predators such as lions, which successfully capture prey in only 9-17 percent of pursuits [10].

Apart from *Ephemeroptera* (Mayflies), Odonata are the only insects that possess flight muscles attached directly to their wings. Smaller insects such as flies and locusts rely on indirect flight; they use muscles attached to the walls of the thorax and flap their wings by compressing their bodies. The method of wing actuation employed by Odonata is more efficient, and enables them to achieve independent control of each their wings. In fact, studies have shown that dragonflies and damselflies employ not only a primary set of flight muscles to flap their wings and produce the flight power required for propulsion, but also a secondary set of smaller flight muscles which independently control the pitch of each wing [11]. Dragonflies are able to generate enormous amounts of propulsive power thanks to the staggering size of their muscles: approximately 40 percent of their body mass can be attributed to flight muscle, as compared to 20 percent for damselflies [12].

Dragonflies are also attractive candidates for study because of the enormous variety of species that exist within the suborder. There are approximately 6000 named species within the order Odonata. The suborder Anisoptera is comprised of three biological superfamilies and ten families, each with distinct biological differences. Species range in size by nearly an order of magnitude, from the tiny *Nannophya pygmaea* (wingspan 26 mm, body length 17 mm) to the massive *Petalura ingentissima* (wingspan up to 160 mm, body length 120 mm) [12]. Dragonflies also vary significantly in flight behavior, ranging from 'fliers' such as *Epitheca cynosure* ("Common Baskettail") which constantly patrol an area and hunt as they fly, to 'perchers' such

as *Pachydiplax longipennis* ("Blue Dasher") which hunt by taking off from perches. Some species of dragonfly have also been known to migrate great distances; a famous example is *Pantala flavescens* ("Globe Skimmer") which has been known to migrate from India to Africa across hundreds of miles of open ocean [12]. Dragonflies of different sizes and flight behaviors likely employ wing designs and kinematics that are optimized for their experience. For example, the aforementioned Globe Skimmer is known to employ gliding kinematics to maximize its aerodynamic efficiency and be able to traverse enormous distances without feeding [12]. Thus, dragonflies provide an opportunity for researchers to determine the differences in flight strategies between various species and be able to use that information to optimize flapping-wing MAV designs to a particular size and mission.

Odonata have an extensive fossil record that goes back to the Paleozoic era, when the ancient tandem-winged *Meganisoptera* with wingspan of length up to 70 cm hunted the skies. Although these insects visually resembled modern-day Anisoptera and had strikingly similar wing planforms, their wings lacked most of the complicated smart structures present in dragonflies [13]. However, smaller contemporary relatives such as the *Eugeropteridae* (which had wingspans of approximately 10 cm) did possess three-dimensional structures in their wings that likely helped induce camber during the wing stroke, as in modern dragonfly wings. By the end of the Mesozoic period, *Odonatoidea* had evolved to utilize modern-day dragonfly wing features such as a leading edge nodus, stiff basal vein complex, and outboard pterostigma. In fact, dragonflies have undergone very little evolutionary change over the last 100 million years. Considering the overwhelming changes undergone by the

vast majority of the animal world during that same period, it can be theorized that dragonflies' wing design and kinematics are optimized for high-performance low Reynolds number flight. These insects have been highly effective predators for millions of years, and as such are prime subjects for bio-inspired MAV designs.

1.3 Flapping-Wing Kinematics

Insect wing kinematics vary between species and have yet to be fully understood for any one type of insect. Nevertheless, certain general kinematics have been determined that apply to the majority of species. An insect's full wing-stroke consists of two half-strokes (a downstroke and an upstroke), each of which contains a translational component and a rotational component. An insect begins its wing stroke with its wings held back above the dorsal region of the body. The wings rotate forward and down about their root attachment point and sweep through the air at a high angle of attack, performing the translational component of the downstroke. As the wings decelerate and reverse direction, they rotate about their spanwise axis to establish a positive angle of attack for the upstroke. This rotational period at the end of the downstroke is called *supination*. The wings are then swept back up to the wing stroke starting point, forming the translational component of the upstroke. As the wings reverse direction to begin a new downstroke, they pitch in the opposite direction as at the end of the downstroke. The adjustment in the angle of attack at the dorsal point of stroke reversal is called *pronation*. As the wings complete each half-stroke, they trace out a stroke plane with their spanwise axis which provides a

reference for the time-history of wing orientation and force production throughout a stroke.

Insects are capable of adjusting many aspects of their wing kinematics either through direct control inputs or indirect changes in aerodynamic or inertial forces. Wingbeat frequency, stroke amplitude, wing velocity, stroke plane orientation, wing pitch amplitude, wing pitch phasing, and deviation from the stroke plane are merely some of the parameters that can vary between insects of different species or insects undergoing different flight modes. In an effort to avoid the inclusion of unnecessary information, detailed discussion will be limited to the current knowledge of dragonfly wing kinematics, as that is the focus of the present work.

1.3.1   Dragonfly Wing Kinematics

The current body of knowledge regarding dragonfly kinematics is extremely lacking, particularly in the case of free-flying studies. One of the first categorizations of free-flying dragonfly kinematics was performed by Ruppell, who used slow-motion footage to determine that typical dragonfly wingbeat frequencies ranged from 35 to 45 Hz, with outliers of 29 Hz for large species (*Tramea lacerate*, 600 mg) and 73 Hz for small species (*Perithemis tenera*, 55.9 mg) [14]. His results showed that dragonflies did not flap their wings at a fixed frequency, but rather showed variability of approximately 37 percent. Ruppell also found several cases of hindwing frequency differing from forewing frequency as the phasing of forewing-to-hindwing flap motion was changed.

Table 1.3: Mean dragonfly kinematic parameters as measured by Wakeling. Values in parentheses indicate minimum and maximum values measured. Values are presented as mean $\pm$ single standard deviation (minimum value, maximum value). Adapted from [15].

Velocity V (m/s)	1.31±0.13	(0.70, 1.66)
Acceleration A (m/s^2)	8.39±2.25	(2.62, 18.33)
Thrust T (mN)	1.93±0.29	(1.11, 3.46)
Mean body angle $\bar{\chi}$ (deg)	29.1±1.97	(22.6, 35.7)
	Forewings	Hindwings
Wingbeat frequency n (Hz)	38.7±0.82	39.2±1.61
	(35.3, 40.8)	(31.6, 44.4)
Stroke plane inclination β (deg)	19.3±2.66	21.1±2.92
	(8.8, 27.9)	(7.0, 28.6)
Stroke amplitude Φ (deg)	90.5±4.95	101.6±3.92
	(64.1, 107.0)	(88.5, 115.8)
Mean elevation angle θ (deg)	17.1±0.61	-3.4±0.82
	(14.7, 19.5)	(-7.2, -1.6)

More detailed dragonfly wing kinematics for flights with linear acceleration were measured eight years later by Wakeling using a film camera recording at 3000 frames per second. Due to being limited to a single camera view, Wakeling was only able to measure kinematics for one forewing and hindwing at a time. A sample of the mean body and wing kinematics measured by Wakeling are shown in Table 1.3. He found that dragonflies of the species *Sympetrum sanguineum* (body mass approximately 120 mg) flapped at a frequency of 38.7±0.82 Hz (with a range of 35.3-40.8 Hz) for the forewings and 39.2±1.61 Hz (with a range of 31.6-44.4 Hz) for the hindwings [15]. A novel result of the Wakeling study was the measurement of the flap and out-of-plane angles of a free-flying dragonfly's wings throughout a wing stroke, as shown in Figure 1.3. We see that the flapping kinematics of the forewing and hindwing are very similar, with a 30 percent phase offset between the two. The out-of-plane angle θ stays below a magnitude of approximately 15 degrees at all times for the hindwing, and varies in such a way that the dragonfly traces a figure-eight pattern with its wingtip during the flapping cycle. This is shown in Figure 1.4, which depicts the dragonfly wingtip trace and stroke plane inclination during the corresponding wing stroke. This figure-eight pattern was found in most of the flights analyzed, although in some the crossover point was located much closer to stroke reversal than mid-stroke.

Additional free-flying kinematics were presented by Li and Dong, who used 3D photogrammetry to track artificial markers placed on the wings of an untethered dragonfly undergoing turning flight [16]. Because of the significantly higher accuracy of the photogrammetry method, they were able to measure detailed stroke, pitch,
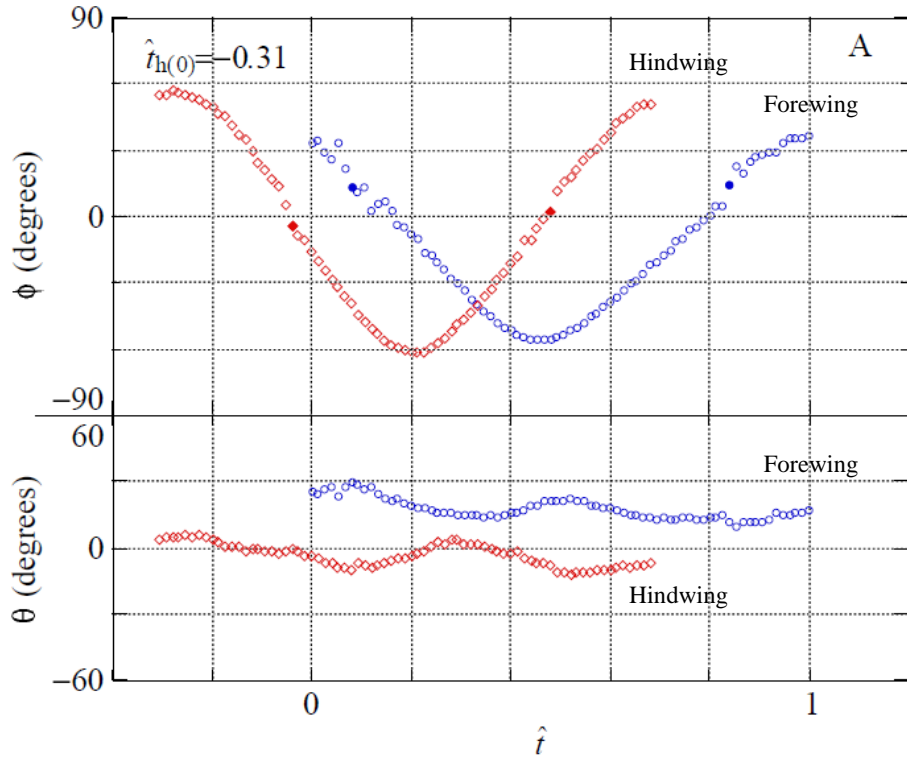
Figure 1.3: Dragonfly wing flap angle Φ and elevation angle θ over a full wing stroke for an unaccelerating flight. Blue markers indicate the forewing and red markers indicate the hindwing. From [15].

and out-of-plane wing angles for all four wings simultaneously over two wing strokes, as plotted in Figure 1.5. By comparing the stroke and pitch angles, it can be seen that the periods of greatest pitch change occurred during stroke reversal. However, the dragonfly did not maintain a fixed pitch during the translational period of the down- and upstroke, but rather continued to rotate its wings throughout the wing stroke. The pitch of the wings does not appear to ever stay fixed, but its rate of change decreases, reaches zero, and reverses sign at a point near the mid-stroke.

14
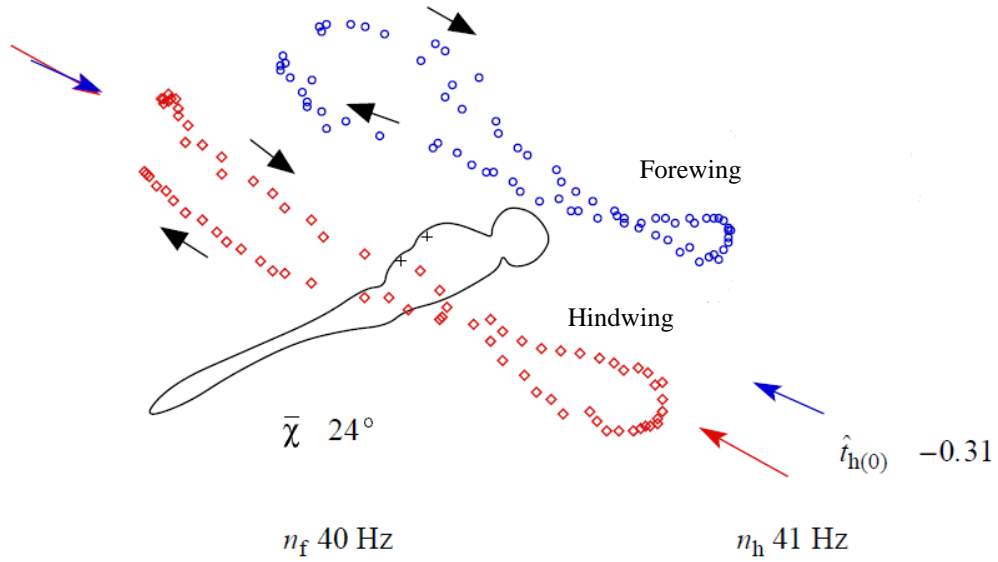
Figure 1.4: Wingtip trace for forewing (blue markers) and hindwing (red markers) corresponding to Figure 1.3. From [15].

1.4 Methodology for Measuring Insect Wing Kinematics

The accurate measurement of insect wing kinematics has presented a daunting challenge to decades of researchers. Insects flap their wings at frequencies high enough that the human eye generally cannot distinguish individual wing strokes, requiring the use of high-speed film to allow any kind of measurements to be made. They tend to avoid maintaining a fixed position or orientation for any substantial length of time, forcing many experimentalists to tether their bodies in order to constrain them to a measurement volume. Finally, their wings undergo simultaneous translation, rotation, and deformation during a wing stroke, further increasing the difficulty of accurately measuring any given parameter.
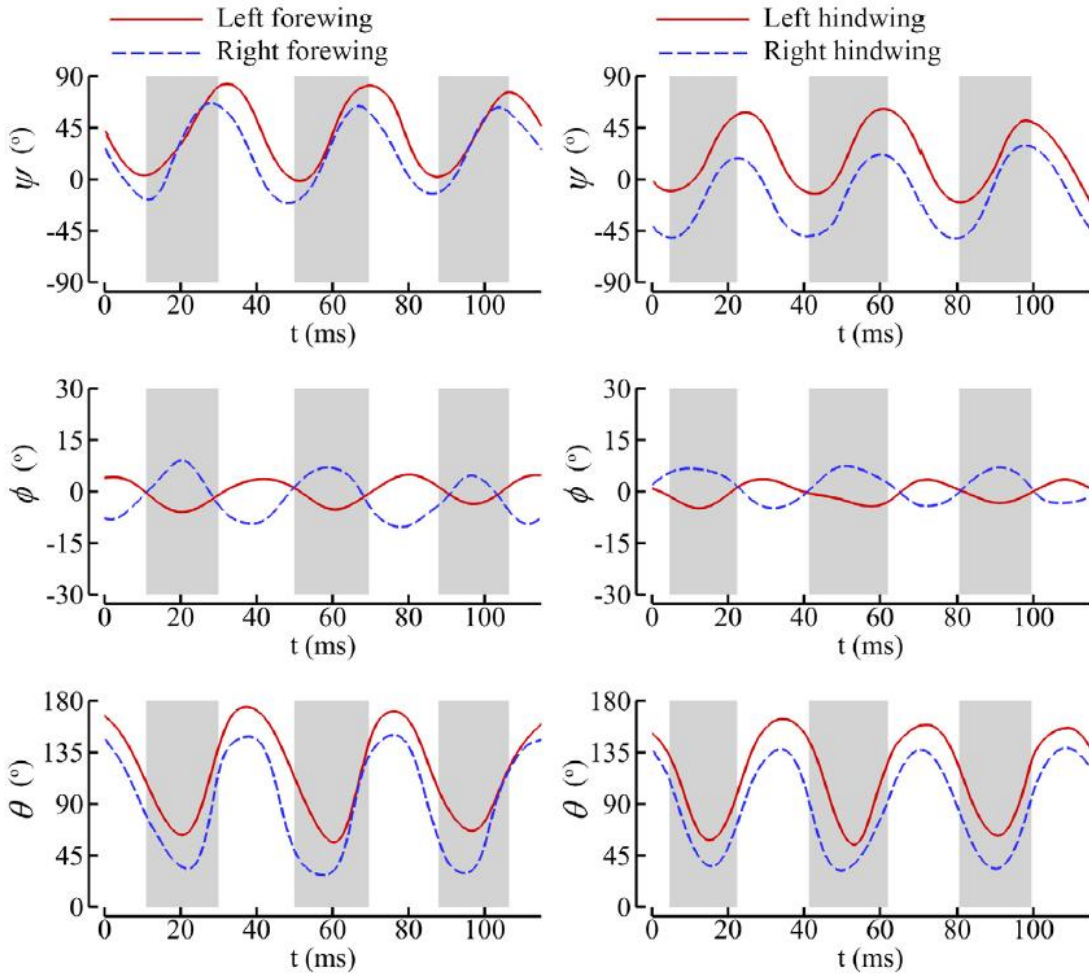
Figure 1.5: Flap angle Ψ, elevation angle ϕ, and pitch angle θ for an untethered dragonfly in turning flight. Shaded regions indicate downstrokes. Note that the flap angle sign convention used here is opposite to that used in this work and in [15]. From [16].

1.4.1 High-Speed Video

Initial attempts to quantify insect wing kinematics involved the use of a single camera to capture high-speed film of their flight. Before the advent of digital imaging, it was nearly impossible to combine detailed quantitative data from multiple

cameras. Thus, early methods were constrained to the use of information from a single imaging plane.

Nevertheless, important initial approximations of basic dragonfly body and wing kinematics were made using this approach. Ruppell collected over 12,000 m of film while capturing high-speed video of various dragonflies and damselflies flying out of a box [14]. He was able use this data to make estimates of various kinematic parameters such as flight velocity, wingbeat frequency, wingbeat phasing, upstroke/downstroke ratio, stroke amplitude, and even angle of attack.

Several studies used single-camera views to provide wingtip traces [17], with more sophisticated experiments making use of projected wing length ratios and manually digitized wing landmarks to calculate stroke plane inclination and geometric angle of attack [15]. However, these methods had suboptimal accuracy due to the inherent limitation of using only one camera view and generally had to assume kinematic symmetry between near and far wing pairs due to optical obstruction [15].

1.4.2 'Strips' Method

A more advanced approach named the 'strips' method was developed which allowed for the measurement of wing angle of attack for free-flying insects [18] using only a single high-speed camera. This technique involves dividing the insect wing into a series of spanwise strips which are free to rotate about the wing's longitudinal axis, as shown in Figure 1.6. For every image frame, the wing outline is manually digitized and an optimization algorithm attempts to adjust the orientation of each
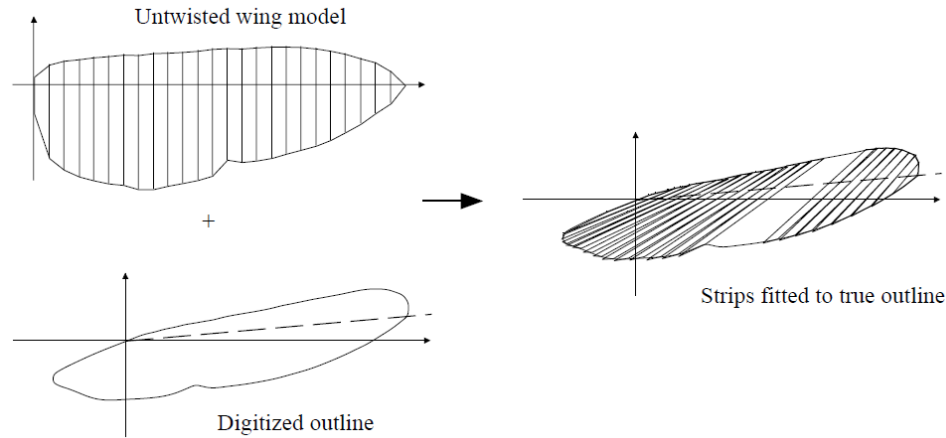
Figure 1.6: Example of 'strips' method applied to an insect wing. From [18].

strip such that the outline of the digital wing model matches the true outline of the wing. The resulting data provide an approximation of the spanwise geometric angle of attack distribution, which can be used as both a measure of the twist of the wing and the wing's overall geometric angle of attack.

This technique does have significant disadvantages, however. It requires manual digitization of the wing outline for every test frame where data are to be collected. Due to the absence of alternative techniques, this amount of manual involvement in the analysis process was acceptable when the 'strips' method was first proposed; in the present day, however, other methods that yield additional data with equal or lesser amounts of human input are preferable.

Perhaps the most significant disadvantage to the strips technique is its inability to account for the presence of camber in the wing. The spanwise strips are assumed to be flat, causing chordwise camber in the wing to be inaccurately represented as spanwise twist [18] [19]. Although it was an advanced method for its time, the

'strips' approach is somewhat outdated today.

1.4.3   Projected Laser-Line

Only a few years later, a new technique was created which was capable of measuring insect wing camber with impressive accuracy. Called the projected comb-fringe method (also known as the projected laser-line method), this approach involved using a laser-based projector to place an array of thin laser lines on the wings of a dragonfly [20]. A single camera was then used to record the distortion of the bright chordwise fringes throughout a section of the wing stroke. Figure 1.7 illustrates the experimental setup used to implement the method, and Figure 1.8 shows examples of the chordwise fringes as captured by a CCD camera. By tracking the deformations of the illuminated laser lines, the camber of the wing can be measured. In addition, the three-dimensional coordinate of any point along each fringe can be calculated if the location of the fringe pattern projector and the imaging camera, as well as the angle of the given fringe, are known. Thus, this method allows for the measurement of both wing kinematics and deformations [21].

The projected laser-line method is one of the most advanced approaches for measuring insect wing kinematics, especially considering that it only requires a single camera to be used. However, it is limited in the amount of detail it can provide by the number of laser lines that can be projected on each wing [19]. In addition, it does not allow for the measurement of data at specific points on the wing due to the fact that the comb-fringe pattern is fixed in space while the insect wing moves
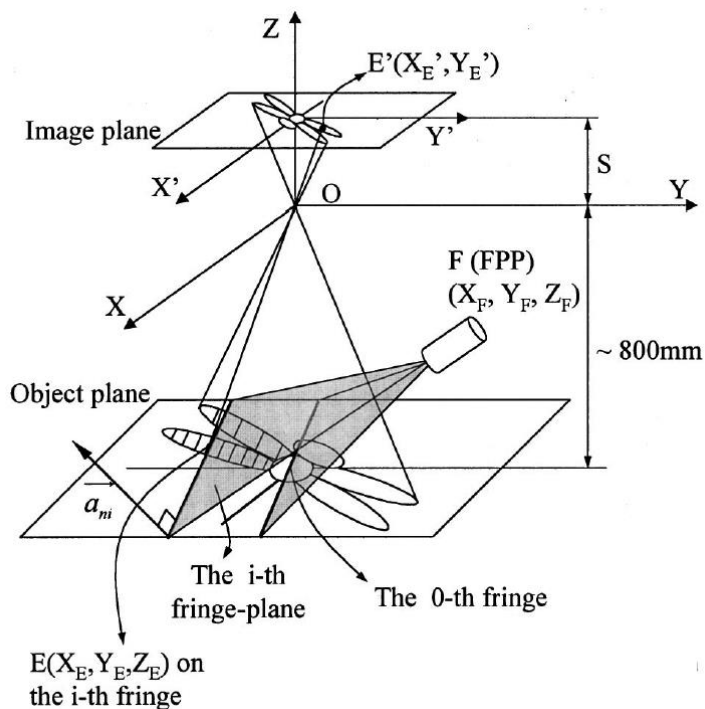
Figure 1.7: Diagram of a projected laser-line system. From [20].

Figure 1.8: Sample test images showing illuminated chordwise lines. From [20].

through it. In the initial development of the method, Song found that because of the angle of the fringe projector and camera, measurements had to be restricted to within 30 degrees of the wing mid-stroke [20]. This also presents challenges with implementing the method for free-flying insects, as the test subjects must fly directly through the small area in which the fringes are being projected. While the method was initially tested on tethered dragonflies [20], it has been successfully used with free-flying insects as well [21]; nevertheless, constraining free-flying insects to small

imaging volumes is very difficult.

1.4.4 3D Photogrammetry

The most recent and advanced technique to be implemented for the measurement of insect wing kinematics and deformations is three-dimensional photogrammetry. This approach is based on a technique that is thoroughly proven and used in a wide range of applications such as cinematography, video game development, and veterinary studies, thanks to the existence of turn-key systems (such as those from Vicon Motion Systems). Photogrammetric systems have routinely been used to measure the kinematics of birds and bats [22], but have only recently been applied to the study of insect wing kinematics [16] [19] [23].

Photogrammetric reconstruction refers to the use of projective geometry to determine the three-dimensional coordinates of a set of points imaged in a spatially calibrated multi-camera system. This technique is much more computationally expensive than those previously discussed, but allows for unprecedented accuracy and resolution in wing kinematic measurement. Although insect flight must occur in a constrained imaging volume, this volume is generally large enough to allow for free-flying subjects. Furthermore, this method allows for specific points on a wing to be tracked throughout an entire wing stroke, a distinct advantage over the projected laser-line method.

1.4.5 Tethered vs. Free-Flight Testing

Many past studies of insect aerodynamics or kinematics have used tethered specimens when testing live subjects. This was done primarily out of necessity; most measurement methods place constraints on the subject that make it impossible to allow insects to fly freely. For example, early force measurement studies of dragonflies required the insects to be physically attached to a force balance in order for data to be collected [24]. Similarly, initial dragonfly flow visualization experiments used tethers to keep the specimen in the camera imaging area [25]. Tethers include rigid struts or loose strings that keep dragonflies from escaping a given test area. They are generally attached to the thorax of a dragonfly through the use of an adhesive.

Although the application of a tether does not directly damage an insect, it introduces several factors into the experiment that can negatively affect the quality of the data, particularly for kinematic investigations. First, the body of the insect will be constrained to a fixed orientation in the case of rigid tethers, and may be angled unnaturally in the case of an insect compensating for a loose tether. Body orientation is an important kinematic parameter for flying insects, and specimens may be forced to alter their wing kinematics in an effort to adjust for an atypical body orientation. Furthermore, even if the body orientation of the insect is correct, the kinematics of their wings while tethered cannot be trusted to accurately represent those used in free flight. Past studies have found that the wingbeat frequencies of tethered locusts were significantly lower than those of free-flying specimens, as
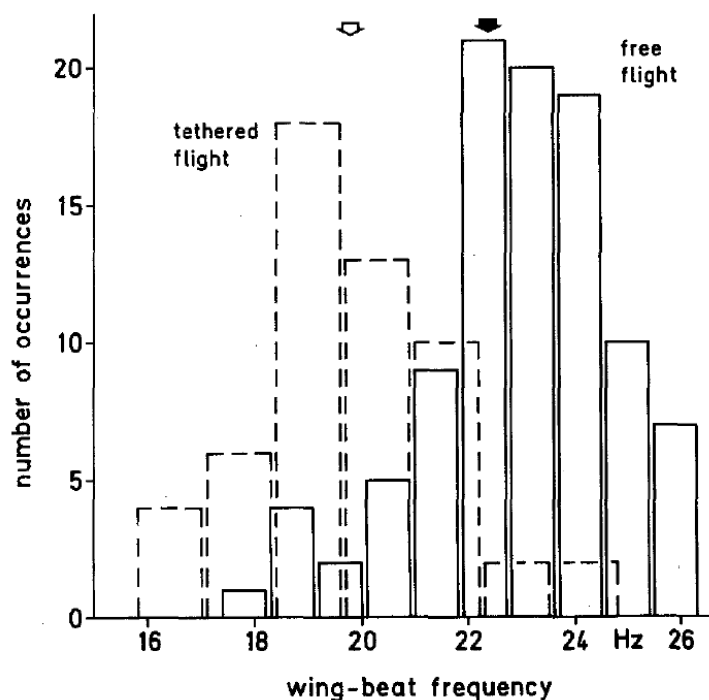
Figure 1.9: Comparison of observed wingbeat frequencies for tethered vs. untethered locusts. From [26].

shown in Figure 1.9 [26]. In addition, substantial discrepancies have previously been noted between tethered and free-flying fly wing kinematics [27].

In the specific case of dragonflies, observations during the course of the present work have shown that Anisoptera have a lack of awareness regarding the fragility of their body and will often cause damage to themselves when trapped or threatened if they are given enough space to do so. Dragonflies have incredibly powerful flight muscles, and could severely injure themselves while trying to escape from a tether.

Therefore, it is preferable to study free-flying specimens whenever possible. A major objective of the present work is to develop an experimental setup that enabled experiments with free-flying dragonfly subjects. Nevertheless, it is recognized that

untethered testing brings additional challenges that cannot be ignored; in some cases, tethered testing is a necessary compromise in order to make the collection of data possible.

1.5 Summary

As interest in developing MAV platforms continues to grow, it is clear that insect-based flapping-wing designs hold much promise as a means of lift and thrust production. Flying insects provide a biological inspiration for these designs, as they have been evolutionarily optimized to fly in the low Reynolds number regime. Dragonflies in particular serve as model candidates for bio-engineered designs due to their incredible aerodynamic performance over a wide range of size scales. Knowledge of dragonfly wing kinematics is limited because of a historical lack of accurate measurement techniques, but recent advancements in the field of three-dimensional photogrammetry have made detailed free-flying wing kinematic studies possible.

1.6 Objective of Current Work

The objectives of the current work are threefold: to first develop an experimental setup that allows for repeated untethered dragonfly flights, to second apply the well-established technique of photogrammetric reconstruction to simultaneously track the position of all four dragonfly wings within a flight, and to finally use the resulting wing position data to calculate detailed kinematic data for a variety of flight maneuvers.

1.7 Outline of Thesis

This thesis began with an overview of the motivation behind the study of drag-onflies as well as a review of the current body of knowledge of free-flying dragonfly wing kinematics and the techniques used to measure them. In order to understand the significance of dragonfly wing kinematics, it is important to establish at least basic knowledge of how certain wing motions relate to aerodynamic performance. To this end, Chapter 2 provides a detailed review of the current understanding of the aerodynamics of flapping-wing flight, with a focus placed on the unsteady aerodynamic mechanisms responsible for lift on insect wings. Chapter 3 gives a thorough explanation of the experimental techniques used to extract kinematic data from flying dragonflies, including the development of a suitable test setup, the implementation of photogrammetric techniques, and the analysis of wing position data. Chapter 4 presents body and wing kinematic results for free-flying dragonflies undergoing a range of flight maneuvers: unaccelerating flight, accelerating flight, climbs, and turns. A brief comparison of the kinematics of three different species of dragonflies is also included. Chapter 5 summarizes the conclusions of the study, and provides recommendations for future kinematic experiments to be undertaken.

Chapter 2:   Flapping-Wing Aerodynamics

2.1   Steady-State Analysis

The aerodynamics of insect flight are complex and challenging to analyze. Researchers have struggled to identify the primary aerodynamic mechanisms involved in flapping-wing flight for over a century. Even today, our understanding of the field is far from complete.

Early work in the subject sought to apply established steady and quasi-steady aerodynamic laws to basic insect wing kinematics. Initial focus was placed on the lift produced by a hovering insect during the translational phase of the wing stroke, in between periods of stroke reversal. During the translational period, the wing appears to hold a relatively steady angle of attack as it rotates about its root attachment point. Thus, it seemed possible that conventional aerodynamic analysis tools could be relevant to the analysis of the translational period of flapping flight.

Initial investigations included the application of thin airfoil theory (and thus the Kutta-Joukowski theorem) to linearly translating insect wings, yielding the classical expression for lift coefficient:

$$C_L = 2\pi\alpha'$$

(2.1)

where $\alpha' = \alpha - \alpha_{L=0}$ is the incidence angle of attack. However, experimental results showed that thin airfoil theory could not fully represent the lift measured for insect wings translated orthogonally to their spanwise direction in a wind tunnel at low angles of attack. An ideal lift curve slope $dC_L/d\alpha'$ has a value of 2π, but this value was found to be 2.2 for a fruit fly wing [28], 4.0 for a crane fly wing [29], and 5.1 for a model locust forewing [29]. Conversely, dragonfly model wings were found to exhibit a lift curve slope of 11 and model pigeon wings were found to have a lift curve slope of 14 [29].

The discrepancies between classical thin airfoil theory and experimental results was primarily attributed to the fact that thin airfoil theory was developed and validated for high Reynolds number flight. The Reynolds number describes the relationship between inertial and viscous forces in a fluid and is defined as:

$$Re = \frac{\rho u L}{\mu} \tag{2.2}$$

Thin airfoil theory had been extensively validated for $Re > 10^5$, but insects flight generally occurs at $Re < 10^4$. The Reynolds number governs flow separation and boundary layer flow, both of which play a vital role in aerodynamic function. Flow separation in particular can negate the applicability of thin airfoil theory because it results in a change to the effective airfoil shape, which classical theory does not account for.

2.2 Quasi-Steady Analysis

Quasi-steady theory was applied to more accurately reflect the aerodynamic forces produced by a wing while undergoing flapping motion. A key assumption made in quasi-steady analyses is that the aerodynamic force coefficients are time-invariant across the wing stroke. These are typically measured on wings in a wind tunnel, where the flow encountered is steady. The influence of unsteady flow effects present during the translational phase of the wing stroke (such as stall avoidance) is accounted for in the measured coefficients due to the analogous nature of the experiments and actual flight. Coefficients corresponding to force production caused by wing rotation at stroke reversal can also be experimentally measured. However, by calculating average force coefficients separately for wing translation and rotation, the unsteady flow effects occurring near periods of stroke reversal are ignored. These include wake capture, added mass, and possibly other unknown flow mechanisms. Lehmann notes that for this reason, early quasi-steady calculations significantly under-estimated the lift coefficients measured for flying insects [30].

Current quasi-steady analyses are capable of providing more accurate estimates of aerodynamic force production by accounting for added mass effects following stroke reversal [31]. However, no reliable wake capture model exists because the related forces are not well understood and are inherently associated with the time history of the flow. Ultimately, quasi-steady models provide a convenient approach for estimating the aerodynamic forces produced by a flapping-wing and can be useful in determining the contribution of lift-enhancing effects that are not included in

the model. Nevertheless, these models cannot provide a comprehensive measure of the aerodynamic performance of a flapping-wing insect or MAV.

2.3   Unsteady Effects: Leading Edge Vortex

As previously mentioned, operating at a low Reynolds number can cause changes in the boundary layer and induce flow separation that would not be seen in the flight regime of large fixed-wing aircraft. Ellington and his contemporaries noted that the insect wings they studied stalled at a much more gradual rate than expected. Flow visualization studies showed a large region of separated flow at the leading edge of the wings, which was determined to be the cause of the delayed stall [29]. Because the flow was observed to reattach itself to the surface of the wing aft of the separation bubble, the primary effect of the bubble was argued to be an increase in camber and thickness for the effective airfoil shape, thus improving aerodynamic performance near stall where the region of separation occurred.

These early studies were a precursor to the discovery of an unsteady flow structure responsible for much of the lift on a low Reynolds number flapping-wing: the leading-edge vortex (LEV). A leading-edge vortex can occur when an airfoil experiences a rapid change in angle of attack or a swift translational acceleration at a high angle of attack, both key components of flapping-wing kinematics. Flow separation at the leading edge can cause a roll-up in the flow on the upper side of the airfoil, creating a vortex. Insect wings are particularly susceptible to flow separation at the leading edge due to their thin profile and sharp edges.

The resulting vortex contains high-velocity flow and thus is a region of low pressure. If the vortex stays attached to the airfoil, meaning that a streamline traveling over it creates a stagnation point on the upper surface of the airfoil behind the LEV, the low-pressure zone serves to increase the lift (and drag) produced by the wing. This increase can be substantial; the difference in lift between initial (LEV present) and steady-state (stalled) values was in one case found to be approximately 200 percent [32].

Leading-edge vortices have also been known to appear on rapidly pitching high Reynolds number airfoils, but are quickly shed into the wake. Therefore, their benefit in this flow regime is minimal, unless the pitching motion is oscillatory in nature (creating the lift-enhancing phenomenon of dynamic stall). However, in insect flight the presence of the LEV is significantly more beneficial because once formed, the vortex tends to stay attached throughout the duration of each half-stroke.

2.4   Unsteady Effects: LEV Stability

Consensus has not yet been reached on what mechanism keeps LEVs attached to the upper surface of insect wings, but a primary suspect is axial flow from the root to the wingtip [33]. This is caused by a multitude of factors, including the presence of the tip vortex and the spanwise pressure gradient due to higher incident velocities at the wingtip than at the wing root. Axial flow can promote leading-edge vortex stability by continuously removing vorticity from the vortex core, preventing the vortex from growing too large and detaching or bursting. It is well-known that

delta-wing aircraft employ axial flow in this manner to maintain leading-edge vortex stability at high Reynolds numbers and increase lift beyond steady values. Although insect wings operate at much lower Reynolds numbers, it is possible that axial flow is responsible for LEV stability here as well.

However, Birch and Dickinson called this theory into question by testing model fruit fly wings fitted with partial chordwise fences to block axial flow [34]. They found no decrease in LEV stability or force production due to blocked axial flow at the leading edge, although they did find that trailing-edge-mounted fences resulted in a 25 percent decrease in aerodynamic force. This suggests that axial flow does not play a primary role in keeping the LEV attached for fruit fly wings, although it is uncertain if this conclusion applies to the wings of larger insects at higher Reynolds numbers. Birch and Dickinson suggested that the combination of the downwash due to lift production and the downward induced flow caused by the tip vortex forms a momentum jet that could serve to inhibit the strength of the LEV and prevent it from growing too large and detaching.

Further doubt was cast upon the axial flow theory by Bomphrey, who used stereo particle image velocimetry (stereo-PIV) to categorize the flow field around the wings of free-flying dragonflies. Although the measurements were limited to periods when the wing was approximately horizontal (i.e. near the mid-stroke point), it was found that spanwise flow velocity along the wing varied in direction and at times was close to zero despite the presence of an attached LEV [35].
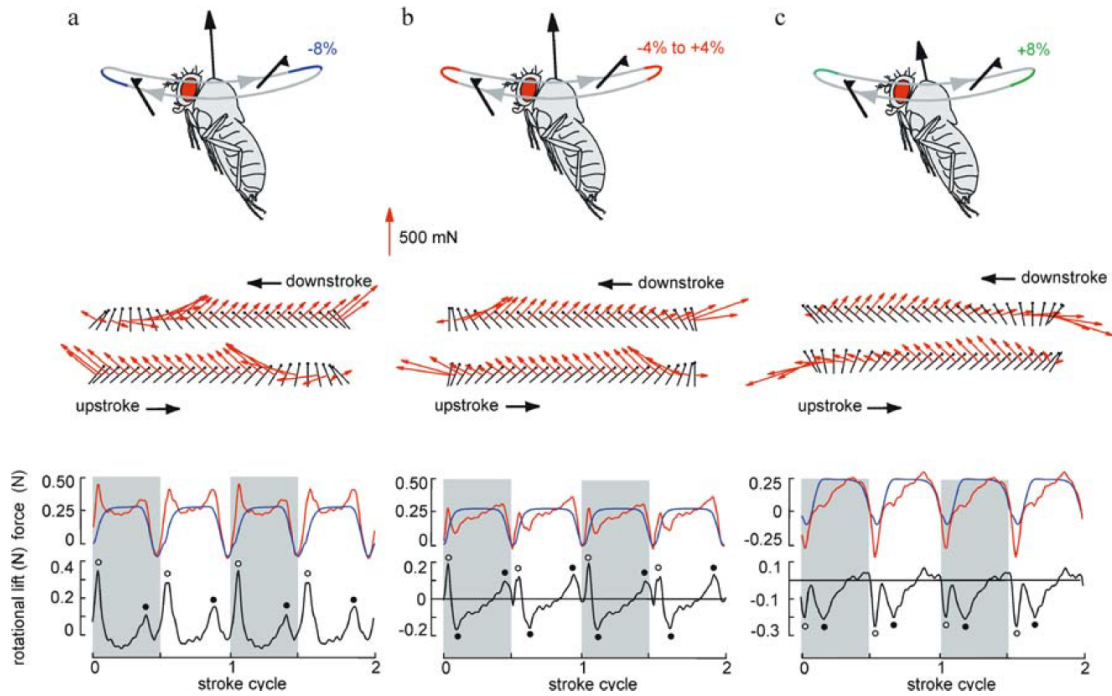
Figure 2.1: Diagram of the kinematics and aerodynamic forces associated with (a) advanced rotation, (b) symmetric rotation, and (c) delayed rotation. From [30].

2.5   Unsteady Effects: Rotational Circulation

Initial studies focused on quantifying quasi-steady aerodynamic forces in the translational phase of the wing stroke, because the periods of rotation during stroke reversal were seen primarily as a kinematic adjustment meant to align the wing to the appropriate angle of attack for the next half-stroke. However, it was recognized that the rotation of the wing must produce some circulation that contributes to the overall lift produced during a wing stroke [29]. It was later discovered that this rotational circulation had a much greater impact than initially believed, causing significant force peaks at the end of each half-stroke [36].

The pitch change of the wing does not occur at rest, but rather during periods of translational deceleration, translational acceleration, or both, depending on how it is distributed over the end of one half-stroke and the start of another. The timing of the rotation has been found to have a profound effect on the overall lift produced during a flapping cycle, as shown in Figure 2.1. Column A depicts *advanced rotation*, occurring entirely at the end of a half-stroke. Here, rotational and translational circulation act in the same direction, complementing each other. As can be seen in the plot of rotational lift in the lower panel, this results in significant lift peaks just before stroke reversal (identified by a solid black dot). Column C depicts *delayed rotation*, in which rotation occurs at the beginning of a half-stroke. Since the rotational circulation acts against translational circulation, we see large negative rotational lift peaks and an overall substantial reduction in the force on the wing. Rotational timing can also occur in between these two extremes, and Lehmann notes that *symmetrical rotation* (column B) has been found to produce only several percent less overall lift than advanced rotation. These studies have made clear that understanding the rotational phasing employed by an insect should be a key goal of any kinematic study.

2.6   Unsteady Effects: Wake Capture and Added Mass

As the wing completes a half-stroke and begins to travel in the opposite direction, it encounters its own wake. This interaction has several profound effects. As mentioned previously, induced flow in the wake may serve a role in limiting the

growth of the LEV and maintaining its attachment. However, the presence of the wake itself can increase lift on the wing through the mechanism of *wake capture* [36]. If the wing is at a positive angle of attack at the beginning of the half-stroke (i.e. if the wing undergoes advanced rotation), the incoming wake will generate a positive lift force as it passes over the wing. If the wing rotation phasing is delayed and the angle of attack is negative at the start of the half-stroke, the transfer of momentum from the wake to the wing will result in negative lift. The forces caused by wake capture in each scenario are shown in the lower panels of columns A and C of Figure 2.1, respectively, and are identified by an open circle. As can be seen, the timing of the wake capture lift peak is independent of rotational phasing, but its sign and magnitude is not. Some computational fluid dynamics (CFD) results have indicated that this lift peak may not be the result of momentum transfer due to wake interactions, but rather an added mass effect caused by the inertial forces of the fluid being accelerated by the wing at the start of the half-stroke [37].

2.7 Tandem Wing Effects

Understanding the aerodynamics of dragonfly flight poses an additional challenge because of their use of tandem wings. Each wing of a dragonfly interacts not only with its own wake but also with the wake produced by the other wings. Dragonflies are able to control each of their four wings independently, allowing for many kinematic combinations of wing stroke phasing.

In straight flight, dragonflies have been found to flap their forewings and hind-

wings approximately 180 degrees out-of-phase with each other when cruising, but flap in-phase during periods of high acceleration [14] [38]. CFD studies have shown that adjusting the phasing of the wings yields large changes to the performance of a dragonfly model; in-phase flapping results in high thrust production but low lift efficiency, while 90 and 180 degree out-of-phase flapping results in lower thrust production but much higher lift efficiency [39] [40]. The loss of propulsive efficiency in counterstroking flight has been attributed to the hindwing extracting energy from the wake of the forewing [39] [6].

Flow visualization studies on tethered and free-flying dragonflies have shown that during counterstroking flight, a leading-edge vortex is present on the forewing while in downstroke, but the flow remains attached during the forewing upstroke and throughout the entire hindwing stroke. Conversely, in-phase stroking produces greater flow separation and results in the presence of a single large LEV attached across both the fore- and hindwings [35] [41]. The large size of this attached vortex is likely responsible for exceptionally high lift coefficients.

Chapter 3: Methodology

3.1   Overview

A custom test environment in which free-flying dragonfly experiments could be conducted was iteratively designed and constructed. A multi-camera setup and three-dimensional photogrammetric techniques were used to reconstruct the spatial coordinates of artificial wing markers. This chapter details the capture and preparation of dragonfly specimens, the test environment design process, the tracking and reconstruction of body and wing marker coordinates, and the kinematic analysis techniques used in the current work.

3.2   Specimen Collection and Preparation

Free-flight experiments were conducted with live dragonfly specimens which were collected in the wild. The photogrammetric technique used for kinematic reconstruction required the presence of markers on the wings of the specimens; thus, each dragonfly had to be prepared for testing.

3.2.1   Specimen Collection

Dragonfly specimens of the Blue Dasher species (*Pachydiplax longipennis*) were collected from Lake Artemesia near the University of Maryland campus with permission from local park authorities. It was observed in the field that male Blue Dashers spent significantly more time on the wing than females, which tended to use their natural green coloration to remain camouflaged among plant life. Males were also significantly more abundant and easier to catch due to their 'percher' nature; they tended to frequently assume a perch, take off to catch passing prey or challenge another male, and return to their perch. Thus, only male Blue Dashers were captured and tested.

Specimens were collected using standard insect nets and immediately placed in folded sandwich bags. The bags were carefully flattened out to fully confine the dragonflies and prevent them from damaging themselves, but were left unsealed to allow air to circulate. It was found that if dragonflies were stored in large containers such as rigid plastic containers, they would continuously attempt to escape by flying into the walls of the container and injure themselves in the process.

The bags were then placed into a small cooler at a temperature of approximately 50 degrees Fahrenheit to slow down the dragonflies' metabolism and prevent them from wasting energy. Once a sufficient number of specimens were captured (generally four to six dragonflies), the insects were brought back to the laboratory.

3.2.2 Species Selection

The Blue Dasher species was chosen for study due to its moderate size, relative abundance, and clear wings which allowed for easy identification of artificial markers. The Blue Dasher has a body mass ranging from 140 to 250 mg and a body length of 28-46 mm. This size is well under the MAV scale limit, but larger dragonflies were not studied for reasons related to experimental setup constraints and ease of capture. First, testing larger specimens would require a physically larger experimental setup. The number of wing strokes that a dragonfly can complete within the imaging volume is inversely proportional to its size; therefore, testing smaller dragonflies allowed for the potential to study multiple consecutive wing strokes. The imaging volume could be made larger, but this would require spacing the cameras further away from the test area, which was not possible due to the geometry of the support structure of the wind tunnel in which tests were held. Second and most importantly, it was observed that large dragonflies were much less abundant than smaller species, and those that were present tended to patrol over the surface of water well out of net's reach.

Blue Dashers were not the only moderate-size dragonfly species present in the local area. Other species included *Tetragoneuria cynosura* (Common Baskettail), *Erythemis simplicicollis* (Common Pondhawk), *Celithemis fasciata* (Banded Pennant), and *Celithemis eponina* (Halloween Pennant). The Banded and Halloween Pennants possess large opaque markings on their wings, making them unsuitable for study. Common Baskettails were much less abundant than Blue Dashers. Common

Pondhawks were easily found in local areas, but tended to perch on water lilies where capture was difficult. Blue Dashers were found to be easier to capture, and thus became the primary test species.

Nevertheless, experiments were done with several other species with the goal of investigating the presence of any differences in their flight kinematics. This thesis will present comparisons of unaccelerating flight kinematics for the Blue Dasher, the Common Pondhawk, and a slightly larger migratory species, the Spot-Winged Glider (*Pantala hymenaea*, body length 43-51 mm, mass 200 mg).

3.2.3 Specimen Preparation

Following capture in the field, the test subjects were transferred out of the cooler and placed in a refrigerator at a temperature of approximately 40 degrees Fahrenheit. It was found that chilling the dragonflies for 30 to 45 minutes slowed down their metabolism enough that they would be completely immobilized for approximately five minutes once they were withdrawn from the refrigerator. This made it possible to place artificial markers on the wings of the dragonflies, the position of which could then be tracked through a multi-camera video sequence and reconstructed using photogrammetric methods.

Fine-tip felt pens were used to apply 30 to 50 circular markers on each wing, as illustrated by Figure 3.1. Approximately six to eight markers were applied to the leading edge of each wing, two markers were placed on the wing tip, at least eight markers were applied to the trailing edge, and the remainder were applied on
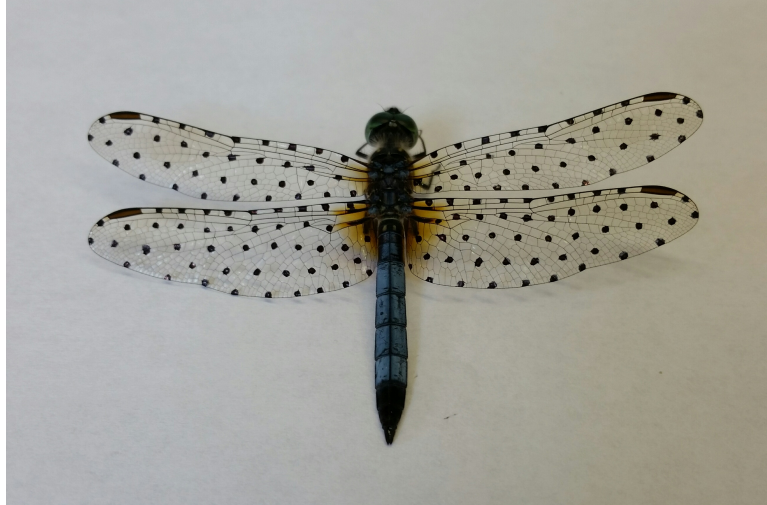
Figure 3.1: An example of a Blue Dasher with artificial markers placed on its wings.

the interior of the wing. The exact number of markers placed on each wing varied according to the area available for marking. Marker spacing was kept dense enough to ensure good resolution for wing reconstruction while still allowing relatively easy marker recognition. Based on previous studies showing that the wing mass of a dragonfly is approximately 2% of its body mass [42], the markers were estimated to weigh less than 2% of the total wing mass for a small (150 mg) Blue Dasher specimen. After the dragonflies were marked, their masses were recorded using a covered laboratory scale and they were placed back into the cooler at 50 degrees Fahrenheit for transport to the test location. Specimens were tested within 2 hours of capture, and released into nature after an average of five tests to prevent exhaustion.

Dragonflies were allowed to warm up for approximately 10 minutes prior to testing. The temperature in the laboratory was kept at approximately 70 degrees, although Blue Dashers appeared to be most active at temperatures above 75 degrees in the field. It is possible that the lower temperature in the laboratory reduced

the frequency of successful flights. It is not known if dragonfly kinematics vary significantly with temperature.

3.3 Experimental Setup

Free-flight experiments were conducted in a custom-built test environment structured around the University of Maryland Autonomous Vehicle Laboratory small-scale wind tunnel. This allowed for testing in both gusting and gust-free environments, although only the latter is detailed in the present work.

3.3.1 Initial Flight Arena Design

Initial tests were attempted in a simple acrylic wind tunnel test section with dimensions of 11.75" by 11.75" by 23.75". Three high-speed cameras were placed above the test section, and three incandescent floodlights were used to illuminate the test section from below. Dragonfly subjects were inserted into the test section and guided onto a bent-wire perch, which they would typically willingly grasp.

The perch was positioned within the camera imaging volume and the intention of the test was to trigger the cameras as the dragonfly took off from the perch, thus capturing high-speed video data of untethered flight. However, the dragonflies proved extremely reluctant to fly of their own volition, often spending up to 20 minutes on the perch without moving. If a subject did move, it generally dropped off the perch and flew upside-down against the bottom glass of the test section, as if it were attracted to the floodlights. Altering the test setup and placing the

floodlights above the test section with the cameras underneath did not remedy the situation. After weeks of testing, the most useful test footage recorded was merely that of a dragonfly warming up its wings with small amplitude fluttering while perched.

3.3.2   Challenges Related to Live Subject Testing

It was clear that working with live insects posed a much greater challenge than expected, and that a new test section design would have to be created that could entice the dragonflies to fly. Prototypes of several different flight arena arrangements were tested to investigate the effect of many different parameters on the dragonflies' willingness to fly.

The greatest success in achieving repeatable free-flight was found when placing dragonflies in a dark tube that led to an open and well-lit enclosure. The dragonflies appeared to be drawn to brightly lit areas, and were observed to periodically fly directly out of the dark tube and continue through the enclosure in a straight line for multiple wing beats. This behavior was far from consistent, but occurred frequently enough to present a strong case for implementing this type of layout in the revised flight arena design. No other test configuration was found to yield a comparable ratio of successful flights.
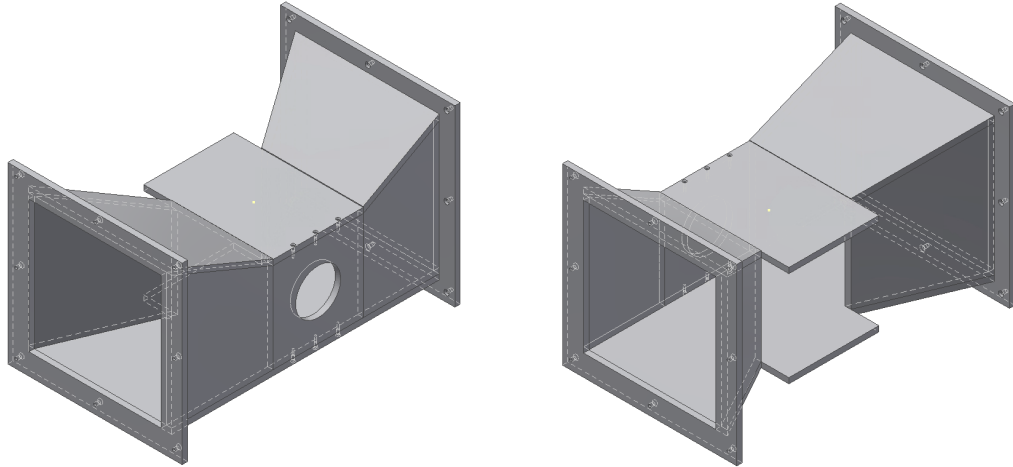
Figure 3.2: CAD model of the revised wind tunnel test section.

3.3.3 Revised Flight Arena

A new, revised test section was constructed for the AVL wind tunnel to accommodate an updated experimental configuration (Figure 3.2). The test section tapered inwards to form an 8" cubic test volume which was initially constrained on its upwind and downwind sides by plastic mesh walls. These were removed following the first round of testing in order to increase the contrast between the dragonfly wing markers and the background, at the cost of allowing the free-flying dragonflies to turn within the test volume and fly into the tapered corners of the test section.

A diagram of the full test system is presented in Figure 3.3. The primary flight arena is contained within the acrylic test section of the wind tunnel, allowing visual access for an array of high-speed cameras placed underneath the enclosure (A). Dragonflies were first placed into a darkened staging tube (B), from which they were encouraged to fly out into the test section by the bright lights illuminating the

43
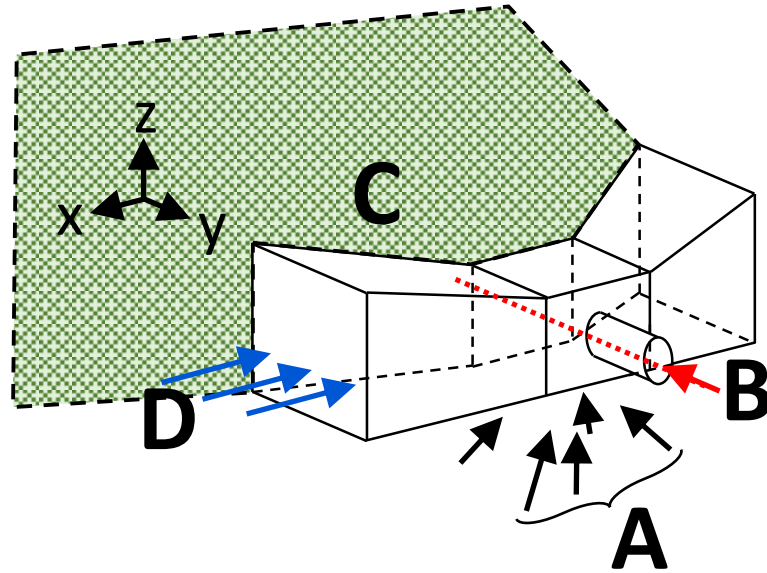
Figure 3.3: Diagram of the revised test set up used to collect free-flying kinematic data.

flight area. The opposite side of the test section was left open to lead into a large mosquito net (C). This allowed the dragonflies to take off from the staging tube, fly directly through the imaging volume in the wind tunnel test section and into the net, from which they could be easily retrieved. The primary advantage of the test environment was the ability of the dragonflies to perform untethered flights while passing through a constrained imaging volume.

3.3.4 Imaging Equipment

Five high-speed cameras were used to record video data of the experiments at 7200 frames per second. The cameras used included various configurations of the Vision Research Phantom v2512, Phantom v710, and Phantom v311, with the v2512 and v710 cameras recording at a resolution of 1280 by 800 pixels and the v311
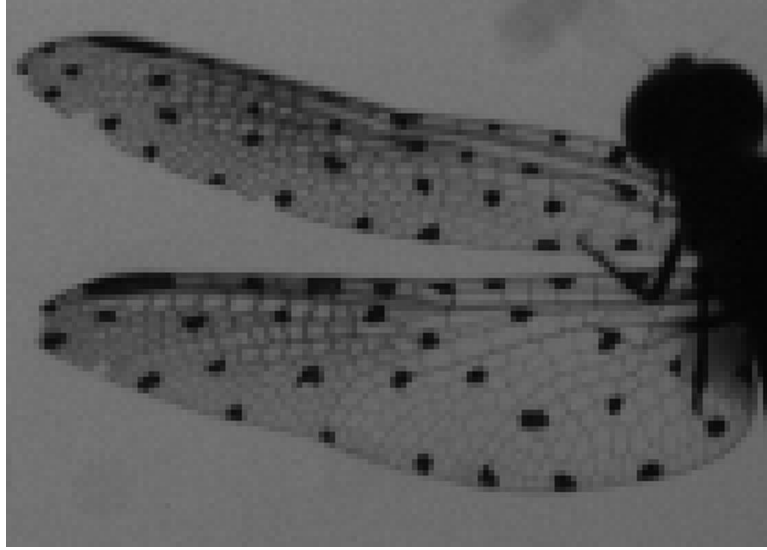
Figure 3.4: A sample test image showing the pixel-level detail measured by each camera.

recording at 768 by 584 pixels. Exposure time was kept at approximately 130 μs, which was sufficient to prevent motion blur effects.

The cameras were arranged underneath the test section with a minimum spacing of approximately 30 degrees, allowing sufficient visual coverage of the wings to track the markers through most test image frames. Increasing the angular spacing of the cameras has a beneficial effect on subject visibility and reconstruction accuracy, but in this case the geometry of the wind tunnel support structure placed constraints on the positions of the cameras. Nevertheless, the camera spacing used was adequate to allow for the markers on all four dragonfly wings to be visible in at least two cameras throughout the majority of the sequence.

3.4 Photogrammetric Methods

3.4.1 Three-Dimensional Photogrammetric Theory

The technique of photogrammetric reconstruction is based on the central perspective projection. Figure 3.5 illustrates this projection for a single camera. A given point of interest in three-dimensional space is depicted as object point X_a. This point has coordinates (X_a, Y_a, Z_a) in a global coordinate system (axes X, Y, Z) that can be arbitrary, but for this work is based on the orientation of the central camera. This object point is projected onto the given camera's imaging plane as image point x_a, with the line X_a-x_a passing through the camera perspective center located at (X_0, Y_0, Z_0). The perspective center lies a distance c away from the projection plane, and the line from the center to the projection plane to the perspective center is called the principal axis. A second coordinate system (axes x, y, z) is defined for each camera with an origin located at the corresponding camera's perspective center. The x and y axes are aligned with the horizontal and vertical axes of the camera projection plane, while the z axis coincides with the principal axis. Thus, the image point on the camera projection plane has the coordinates $(x_a, y_a, -c)$ in the image coordinate system.

The photogrammetric model is described by the collinearity equations as defined in [43]:

$$x_a = \frac{-c[r_{11}(X_0 - X_A) + r_{12}(Y_0 - Y_A) + r_{13}(Z_0 - Z_A)]}{[r_{31}(X_0 - X_A) + r_{32}(Y_0 - XY_A) + r_{33}(Z_0 - Z_A)} \tag{3.1}$$
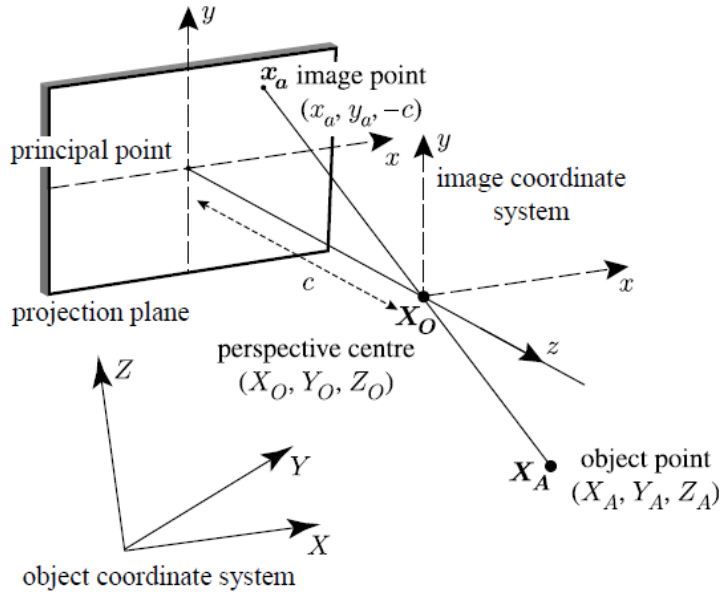
46

Figure 3.5: Illustration of the projection model used for photogrammetric reconstruction. From [19].

$$y_a = \frac{-c[r_{21}(X_0 - X_A) + r_{22}(Y_0 - Y_A) + r_{23}(Z_0 - Z_A)]}{[r_{31}(X_0 - X_A) + r_{32}(Y_0 - XY_A) + r_{33}(Z_0 - Z_A)} \quad (3.2)$$

These equations relate the object coordinates (X_a, Y_a, Z_a) to the corresponding image coordinates (x_a, y_a) through the use of the rotational matrix R which transforms the the object coordinate system to the image coordinate system. Equations 3.1 and 3.2 also require the principal axis distance c to be known, as this is the z-coordinate of the image point in the camera frame. According to these equations, each image point can be considered to create a line in three-dimensional space when it is reprojected from the projection plane through the perspective center.

When a system of m cameras is used to track n image points, the equations

become generalized for each camera k and image point i:

$$x_{i,k} = \frac{-c_k[r_{k,11}(X_{0,k} - X_i) + r_{k,12}(Y_{0,k} - Y_i) + r_{k,13}(Z_{0,k} - Z_i)]}{[r_{k,31}(X_{0,k} - X_i) + r_{k,32}(Y_{0,k} - Y_i) + r_{k,33}(Z_{0,k} - Z_i)} \qquad (3.3)$$

$$y_{i,k} = \frac{-c_k[r_{k,21}(X_{0,k} - X_i) + r_{k,22}(Y_{0,k} - Y_i) + r_{k,23}(Z_{0,k} - Z_i)]}{[r_{k,31}(X_{0,k} - X_i) + r_{k,32}(Y_{0,k} - Y_i) + r_{k,33}(Z_{0,k} - Z_i)} \qquad (3.4)$$

The three-dimensional coordinates of object point X_a can then be calculated by solving the resulting system of collinearity equations. This can be visualized as finding the intersection point of a series of three-dimensional lines generated by reprojecting the image points from each camera projection plane. In practice, no exact solution is possible due to inherent measurement errors in the optical system. Instead, the system of equations becomes a minimization problem where the distance between each reprojected line and the estimated object point coordinates is minimized. Thus, the result is an estimate of the object point coordinates, the accuracy of which increases as more cameras are introduced into the system.

3.4.2   Camera Calibration

Knowledge of camera parameters c and R is essential to solving the collinearity equations. Thus, calibration is required to calculate these parameters for each camera and allow for photogrammetric reconstruction to be performed. A bundle adjustment technique ([43], [44]) was used to calibrate the system of cameras and provide estimates of the camera parameters. This technique is preferred over other techniques such as Direct Linear Transformation (DLT) because it does not require the knowledge of the relative three-dimensional positions of object points during
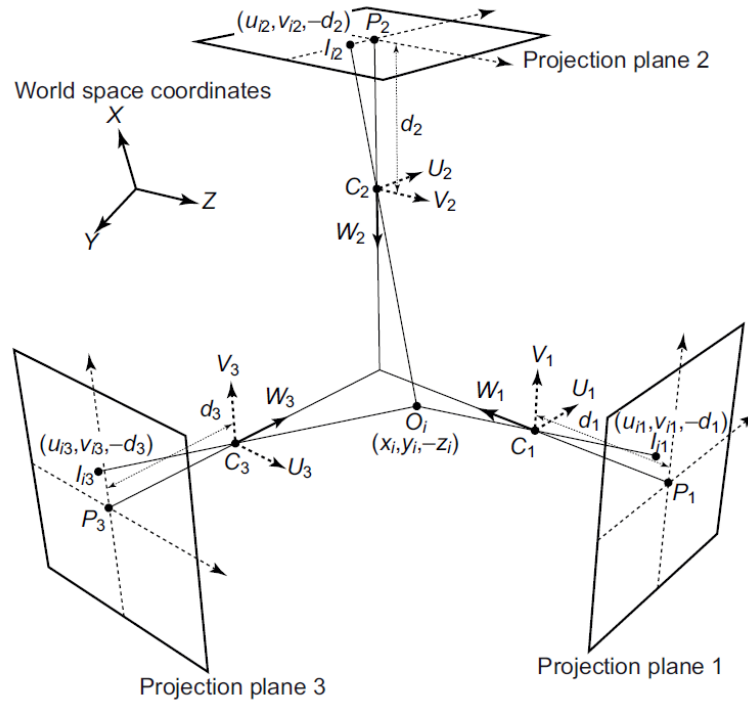
Figure 3.6: Diagram of the central perspective model implemented for a system of cameras. From [23].

calibration. Photogrammetric studies using DLT techniques have used high-detail 3D printed solids with reference markers arranged on their surface as calibration objects [23]. Conversely, bundle adjustment techniques require only a simple 2D grid of circular markers with known spacing. The calibration object is then used to produce reference images that allow for the calculation of the camera parameters. A detailed description of the bundle adjustment calibration procedure can be found in [19]. Walker et. al. have made their bundle adjustment software freely available, and it has been used to calibrate the system of cameras used in the present work.

Optical distortion effects such as lens offset and lens distortion were assumed to be negligible based on validation experiments conducted on insect-oriented pho-

togrammetric studies in the past [19] [23]. Mean reprojected pixel error (RPE) values during calibration were approximately 0.1 pixels. It was found that if the image-coordinate position of a marker had an error of 1 pixel in every camera, the resulting three-dimensional position error after photogrammetric reconstruction was about 0.1 mm.

Approximately thirteen calibration images were taken with a calibration grid placed in the imaging volume with systematically varying orientation. Calibration was performed whenever any component of the optical system was altered; this included new cameras being introduced into the system and any changes being made to the focus or aperture of the camera lenses. In order to account for unexpected disturbances to the alignment of the camera system, calibration was also performed every other test day even when no changes had been made to the system.

3.5   Body and Wing Marker Tracking

3.5.1   Dragonfly Body Tracking

The first step of the analysis process involved collecting bulk body kinematics by fitting a geometric model of a dragonfly body (as illustrated by Figure 3.7) to the image of the specimen in each camera view and frame. The body model fitting software used was created by Nathan Shumway of the University of Maryland. For every frame in the sequence, the body model was placed in an initial position and various parameters were iteratively adjusted until an optimal fit was found. This resulted in the generation of three-dimensional body position and orientation
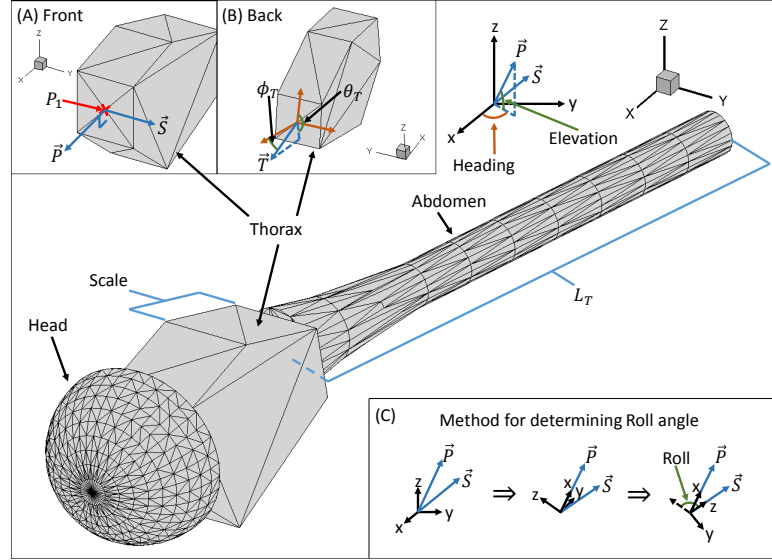
Figure 3.7: The geometric model fitted to the silhouette of the dragonfly at every frame for the collection of body kinematics.

data for the duration of this sequence. The body model was projected onto the test sequence images and optically verified to be qualitatively accurate in its scale, position, and body orientation angles.

Some difficulty was encountered in the estimation of the roll orientation of the dragonfly due to the symmetry of its body about the longitudinal axis. Asymmetries in the geometry of the thorax did make the estimation of the roll angle possible, and the resulting data were generally found to be optically accurate. Nevertheless, errors in the roll angle of up to 30 degrees are possible. Therefore, conclusions drawn from kinematic parameters that depend strongly on the body roll angle (namely, the in-stroke wing elevation angle and the stroke plane inclination angle with respect to body axes) were limited. Key kinematic parameters such as wing stroke duration, phasing, amplitude, wing flap angle, and wing pitch angle are not strongly affected

by discrepancies in the body roll angle.

3.5.2   Wing Marker Tracking

Once body kinematic data were available, wing marker tracking was performed using a custom-written semi-automated MATLAB routine. This software was created by Nathan Shumway with assistance from the author. Due to the high number of markers visible in each frame, automatic tracking was essential for maintaining acceptable analysis time. Nevertheless, optical issues such as body obstruction and wing overlap made partially manual analysis unavoidable. Not all markers were identified for every frame, but due to the amount of markers placed on each specimen there were almost always sufficient data for the calculation of wing kinematics.

Although the marker tracking software was designed to be primarily automated, the level of operator involvement required for successful data acquisition remained high. A trained worker is capable of using the marker tracking program to extract marker position data at an average of ten frames each hour. This rate is highly dependent on wing visibility, and ranges from 5 frames per hour for periods of extensive wing overlap to 80 frames per hour during low-flapping-frequency flight where the wings are not obscured. Over 6300 frames of marker data were extracted from twelve separate flights, representing nearly six months of half-time work for two operators.

3.5.3 Marker Data Smoothing and Accuracy

Three-dimensional global marker position data were transformed into a body-centered set of coordinate axes (P, S, T) as defined in Figure 3.7 and smoothed using previously developed code which utilized third-order spline fits. The time histories of the smoothed position data for each marker were verified against the raw data, and erroneous sections were either manually adjusted or eliminated.

The accuracy of the photogrammetric reconstruction was verified by attaching a marked dragonfly wing to a 3-axis linear stage and comparing the actual distances traversed to the average marker displacements found using the marker tracking code. Using unsmoothed marker data resulted in an average three-dimensional displacement error of 0.1 mm. This value was similar to those found in previous insect-based photogrammetric studies [16] [19]. The wing was also pitched using a rotational stage. The mean error found in the pitch angle of the wing was approximately 2.5° during times of small pitch change and 5° during periods of greater pitch change when marker visibility suffered due to poor alignment of the wing with respect to the cameras.

Minimal smoothing was performed on the final kinematic data presented in Chapter 4. A simple 8-point moving average was applied to smooth out small (1-2°) discontinuities caused by the periodic loss of position data for certain wing markers which were incorporated into the wingtip direction vector. Certain sections where data were scattered due to nearly all of the wing markers not being visible were manually removed. However, this was done very rarely. The missing sections of

kinematic data seen in Chapter 4 were primarily caused by a failure to identify an accurate wingtip vector due to poor marker visibility.

3.6   Kinematic Analysis

3.6.1   Kinematic Parameter Definitions

Wing kinematic motion was described using two primary parameters, as defined in Figures 3.8 and 3.9. The flap angle ϕ of each wing was defined as the angle between the projection of the wingtip line onto the stroke plane and the mid-stroke line of the corresponding half-stroke. Following the convention used in [15], positive values of ϕ indicate that the wing is closest to the point of pronation, while negative values of ϕ indicate that the wing is closer to the point of supination. Thus, a downstroke begins at a positive flap angle and ends at a negative value. The stroke amplitude ϕ_{tot} was calculated as the difference between the maximum and minimum flap angles for a given half-stroke.

The wing geometric pitch angle θ was defined as the angle between the wing plane and the stroke plane after the wing vector was aligned with the mid-stroke axis using the methods described in the following section. The pitch angle was calculated according to right-hand convention as in [16], resulting in positive angles throughout the wing stroke. This meant that the wing was expected to have a pitch angle between 0 and 90° during the downstroke, and between 90 and 180° during the upstroke.
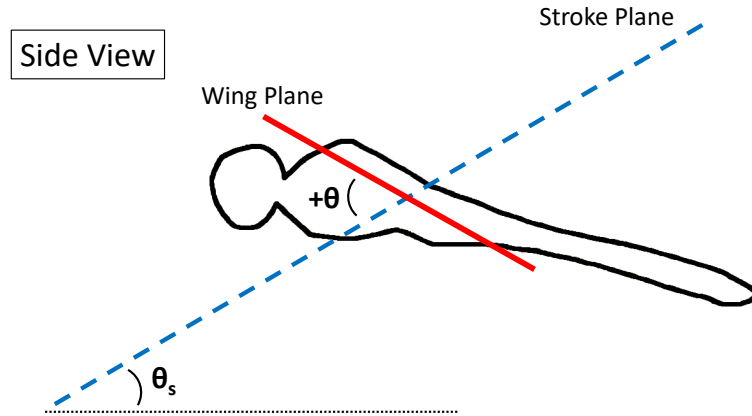
Figure 3.8: Side view of a dragonfly body model, illustrating the definition of the wing geometric pitch angle θ.
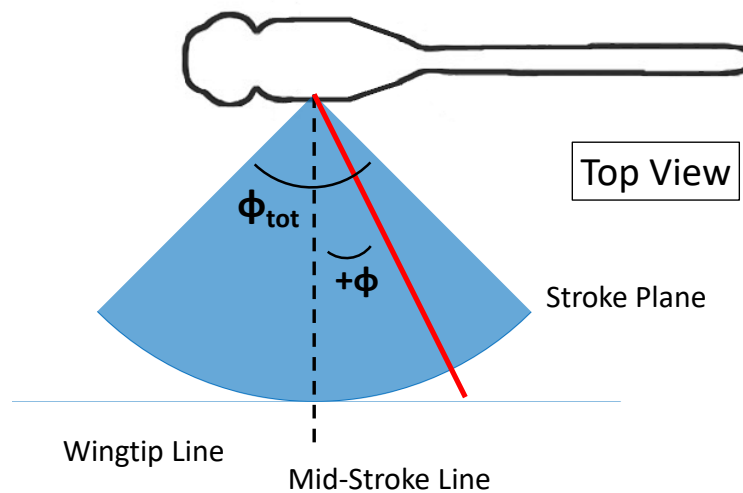

Figure 3.9: Top view of a dragonfly body model, illustrating the definition of the wing flap angle ϕ. Note that the flap angle is positive when the wing is aft of the mid-stroke line in the body frame.

3.6.2   Calculation of Kinematic Parameters

The bulk motion of each wing was approximated by fitting a least-squares plane to the available marker position data for each frame. This approximation prevented

wing deformations from being modeled, and the presence of any deformations of the wing (most commonly, twist at the wingtip) contributed to minor errors in the kinematic wing angle calculations. Marker points found to be more than 5 mm away from the wing plane were treated as erroneous and were not considered for the final plane fit. The motion of the wing plane was then tracked in the body coordinate axes (P, S, T) as defined in Figure 3.7. Wingtip marker positions were traced throughout each sequence in order to identify stroke reversal points (i.e., points of pronation and supination). These points were used along with the respective wing root point in order to define a stroke plane for each half-stroke of the wing.

Four markers comprising a line between the wing root and the wingtip marker were selected for each wing to define a wingtip direction vector that could be tracked even if data were not available for the wingtip marker itself. For every frame, this wingtip line was projected onto the stroke plane and the flap angle was calculated as the angle between the wingtip line projection and the mid-stroke line. The wingtip vector (and the wing plane normal vector) were then rotated by this angle around the stroke plane normal axis to place the wingtip vector within the plane drawn by the mid-stroke line and the stroke plane normal axis. The angle between the wingtip vector and the mid-stroke line was calculated as the elevation (or out-of-plane) angle, and the wingtip and wing plane vectors were rotated about the cross product of the mid-stroke and stroke plane normal lines in order to align the wingtip vector with the mid-stroke line. At this point, the wing plane normal vector became entirely perpendicular to the mid-stroke line, and the pitch angle was found as the angle between the wing plane and stroke plane normal vectors.

Although the time history of the elevation angle was found for every test, only the flap and pitch angle data will be presented due to uncertainties regarding the accuracy of the body roll angle estimate provided by the body model and the direct dependence of the elevation angle on the roll angle of the dragonfly.

Chapter 4:   Results and Discussion

4.1   Overview

More than one thousand free-flight tests were performed over the course of two summers. Data was saved for 669 of the trials, with 295 representing non-gust tests. Approximately half of the attempted trials resulted in the dragonfly falling out of the staging tube into the test section, flying against the test section walls, or otherwise not engaging in useful flight within the imaging volume. Table 4.1 describes the number of tests in which data were recorded for each species of dragonfly.

Of the 295 gust-free tests where data were kept for initial analysis, approximately 10 were reasonably straight flights that were well-suited for additional analysis. Several other tests included various accelerations and maneuvers that made them suitable for study. However, the majority of the recorded tests were limited in usefulness due to poor flight patterns or compromised visibility. For example, in many tests the dragonfly flew through the corner of the imaging volume and an insufficient amount of data were recorded for kinematic analysis. Due to the time-intensive nature of the marker data extraction process, only twelve individual runs were selected for complete analysis. These represent four types of maneuvers:

1. Straight, unaccelerating flights: Flights 1-4

2. Accelerating (diving) flights: Flights 5-6

3. Climbing flights: Flights 7-8

4. Turning flights: Flights 9-10

In addition, one unaccelerating flight each of a Common Pondhawk and a Spot-Winged Glider were fully analyzed to investigate any significant kinematic differences between these two species and the Blue Dasher. This chapter contains separate sections for each of the five flight comparisons. All sections follow a similar format, with individual body and wing kinematic data presented for every flight. Body kinematic data include three-dimensional positions, orientations, and bulk velocities. Wing kinematic data focus primarily on stroke amplitude, wing phasing, wing pitch values throughout the stroke, and the relationship between flapping and pitching motions. The masses of the specimens for each tests are presented in Table 4.2.

Table 4.1: Total number of tests where data were acquired for each dragonfly species.

Dragonfly Species	Number of Tests
Blue Dasher	221
Common Pondhawk	68
Spot-Winged Glider	3
Slaty Skimmer	3
Total	295

Table 4.2: Masses of dragonfly specimens for Flights 1-12.

Flight Number	1	2	3	4	5	6
Dragonfly Mass (mg)	153	220	153	231	178	262
Flight Number	7	8	9	10	11	12
Dragonfly Mass (mg)	231	129	164	234	219	197

4.2 Unaccelerating Flights

Four straight, level, and reasonably unaccelerating flights were analyzed to determine standard wing kinematics in cruising flight and investigate the level of kinematic variability between similar flights. The four flights chosen for kinematic analysis were the most turn-free, level, and constant-speed of the flights categorized as "straight" based on video data. The body kinematic data are presented in Figures 4.1 and 4.2. The upper left plots depict the path of the dragonfly in the global x-y plane, with the x-direction corresponding to the longitudinal axis of the staging tube and the y-direction corresponding to the longitudinal axis of the wind tunnel. All four flights were free of turns. Flights 1-3 involved the dragonfly flying directly through the imaging volume from the staging tube into the mosquito net, while Flight 4 was recorded later in the course of a test after the dragonfly had made a turn.

All four flights exhibited minimal changes in vertical position. Flights 2 and 4 included minor climbs near the end of the sequence, but kinematic data were
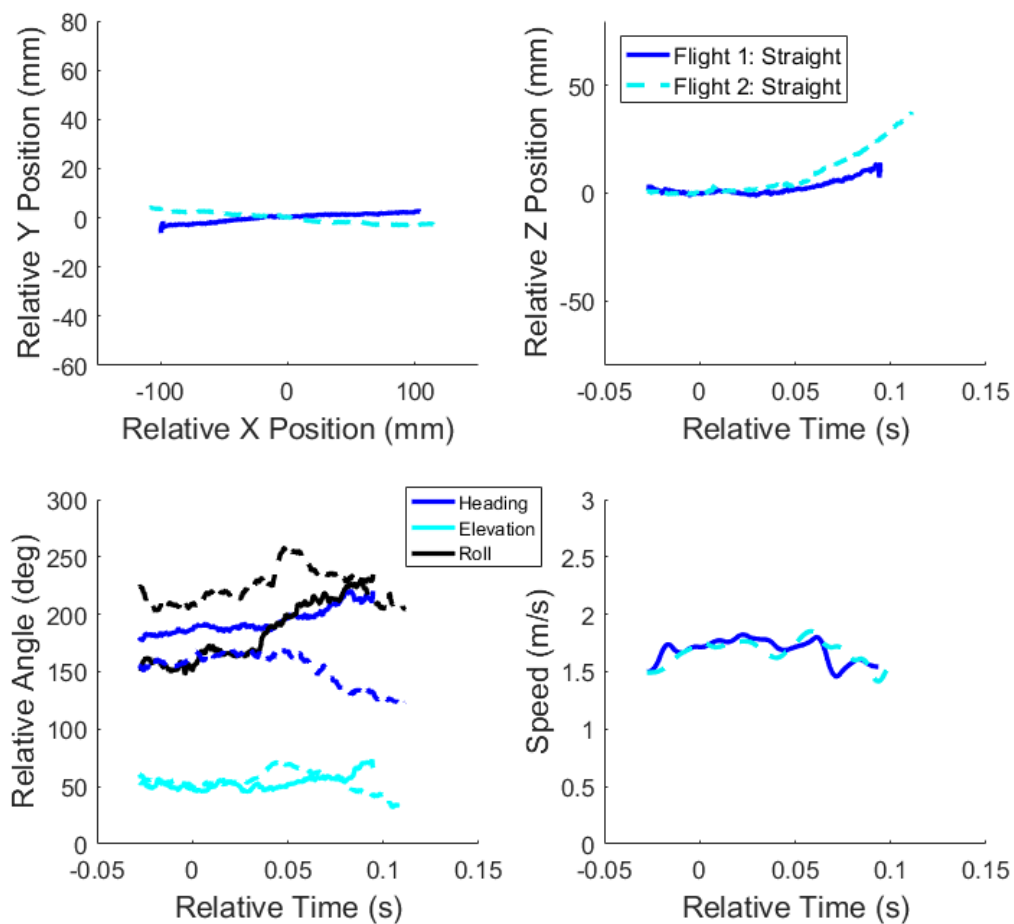
Figure 4.1: Body kinematic data for Flights 1 and 2.

drawn primarily from the earlier portions of the tests. Flight velocities aligned extremely well for Flights 1 and 2, with both dragonflies flying at approximately 1.7 m/s. Flight 3 was slightly faster than this at 2 m/s, while Flight 4 was slower at approximately 1.3 m/s.

The most prominent body kinematic differences between the four tests appeared in the orientation angles. Although Flights 1-3 were all in the same direction, the dragonflies exhibited substantial variation in their heading angles. The
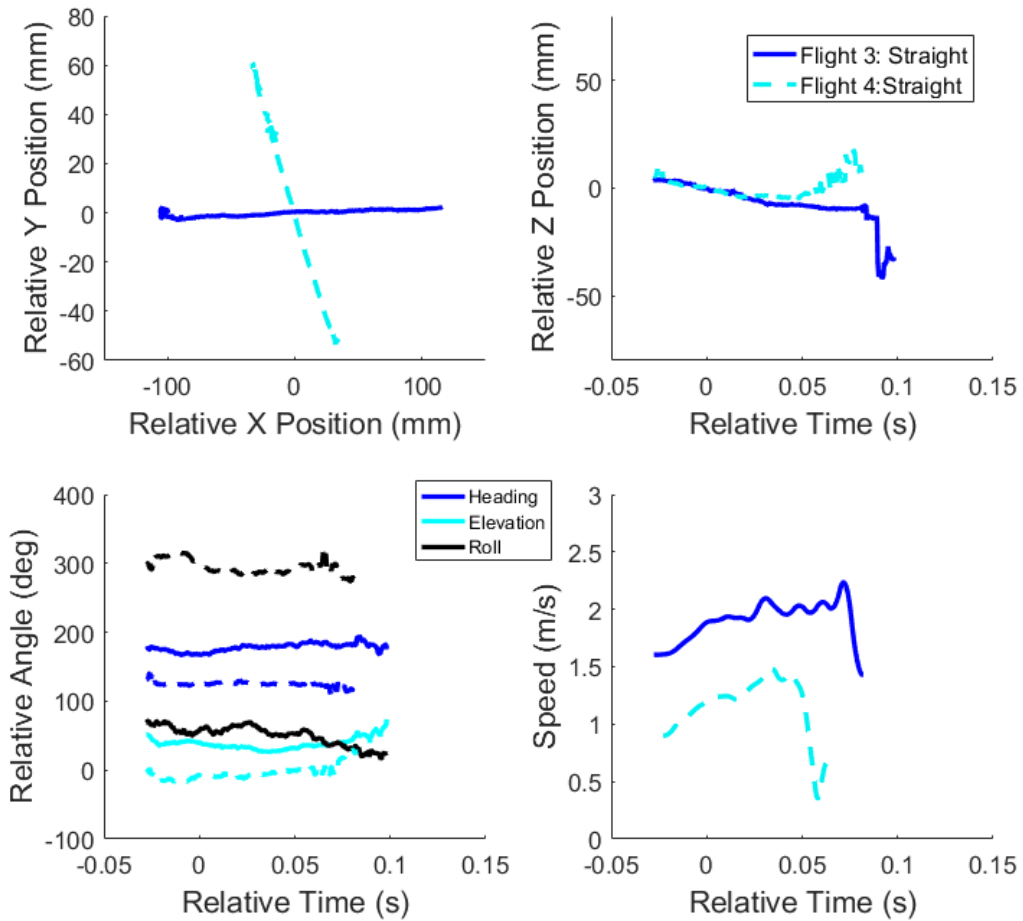
Figure 4.2: Body kinematic data for Flights 3 and 4.

dragonfly in Flight 1 began by pointing its body in the direction of its velocity, but yawed significantly during the last half of the flight to end up pointing about 40° off of its velocity vector. Flight 2 involved a similar maneuver in the opposite direction, while the test subject in Flight 3 kept its body closely aligned with the velocity vector at all times. The dragonflies tended to keep their bodies pointed upward approximately 50° off of the horizontal plane, but the dragonfly in Flight 4 maintained a near-zero degree (and sometimes slightly negative) body elevation

angle.

The wing kinematic data also exhibited substantial amounts of variability, although several consistent trends were observed. All four flights displayed in-phase flapping and pitching between the forewings as well as between the hindwings. The motion of the forewings and hindwings was never observed to be in-phase, but instead the forewings always lagged behind the hindwings. The phase differences between the forewings and the hindwings were 94°, 98°, 93°, and 75° for Flights 1-4 respectively, with an average value of 90°. As expected, there was generally a high degree of symmetry between left and right wing pairs. The flapping motion typically followed a sinusoidal profile, although a surprising "two-step" upstroke profile was observed on two occasions: first for the left forewing of Dragonfly 1 (Figure 4.3) and again for the right forewing of Dragonfly 2 (Figure 4.4). This could be indicative of a change in the flow structure of the forewing at mid-upstroke, which could serve to briefly slow the flapping motion of the dragonfly. In the case of Flight 2, this change in flap profile actually results in the right forewing moving out-of-phase with the left forewing. The two-step flap angle profile was not observed for any other tests except for the unaccelerating flight of the Spot-Winged Glider (Flight 12). The stroke amplitudes were found to be approximately 95° for both forewings and the right hindwing, but 105° for the left hindwing. This difference is within the standard deviation of the hindwing stroke amplitudes, and is not likely to be significant. The stroke amplitude values ranged from 79° to 130° despite a lack of overt maneuvers, suggesting that dragonflies may significantly alter their stroke amplitudes to adjust their trim conditions. Similar variations in stroke amplitude
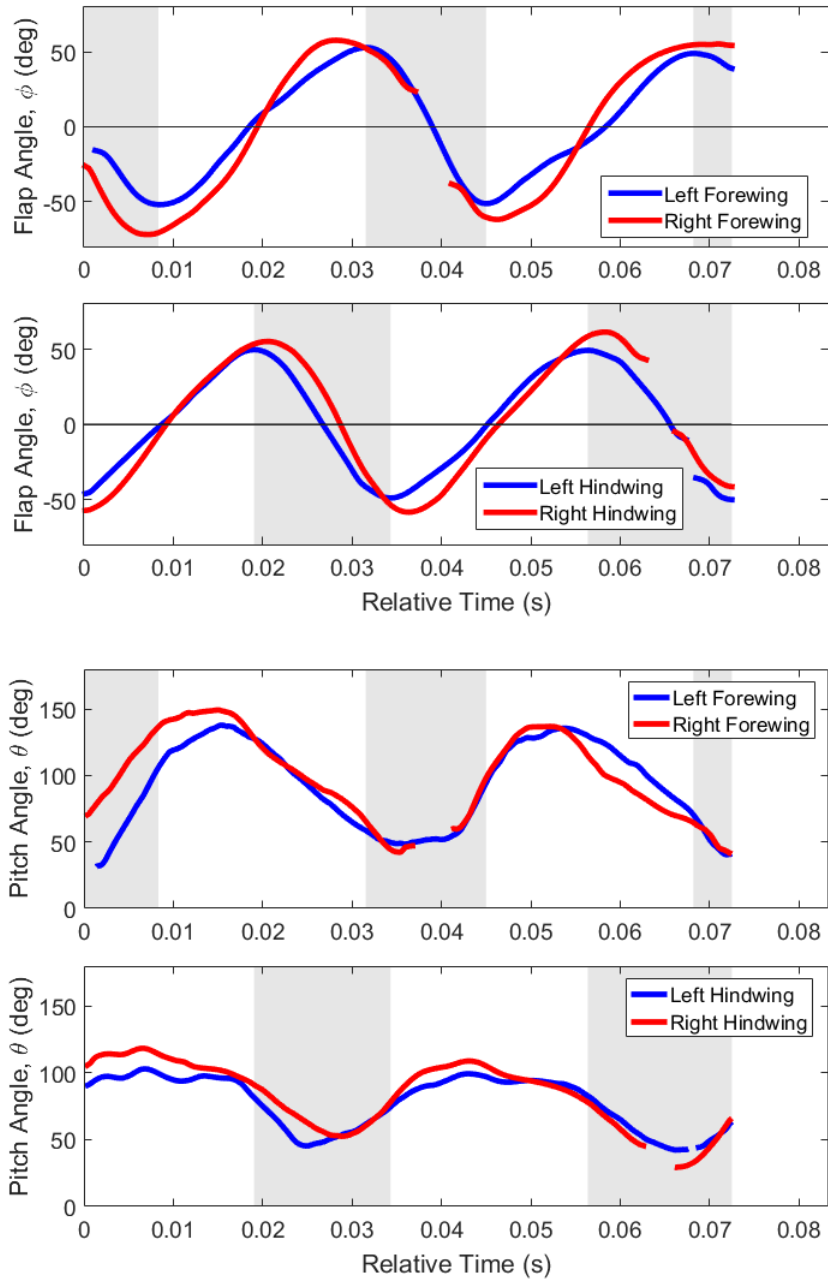
63

Figure 4.3: Flap and pitch angles for Flight 1. Shaded regions indicate downstrokes.
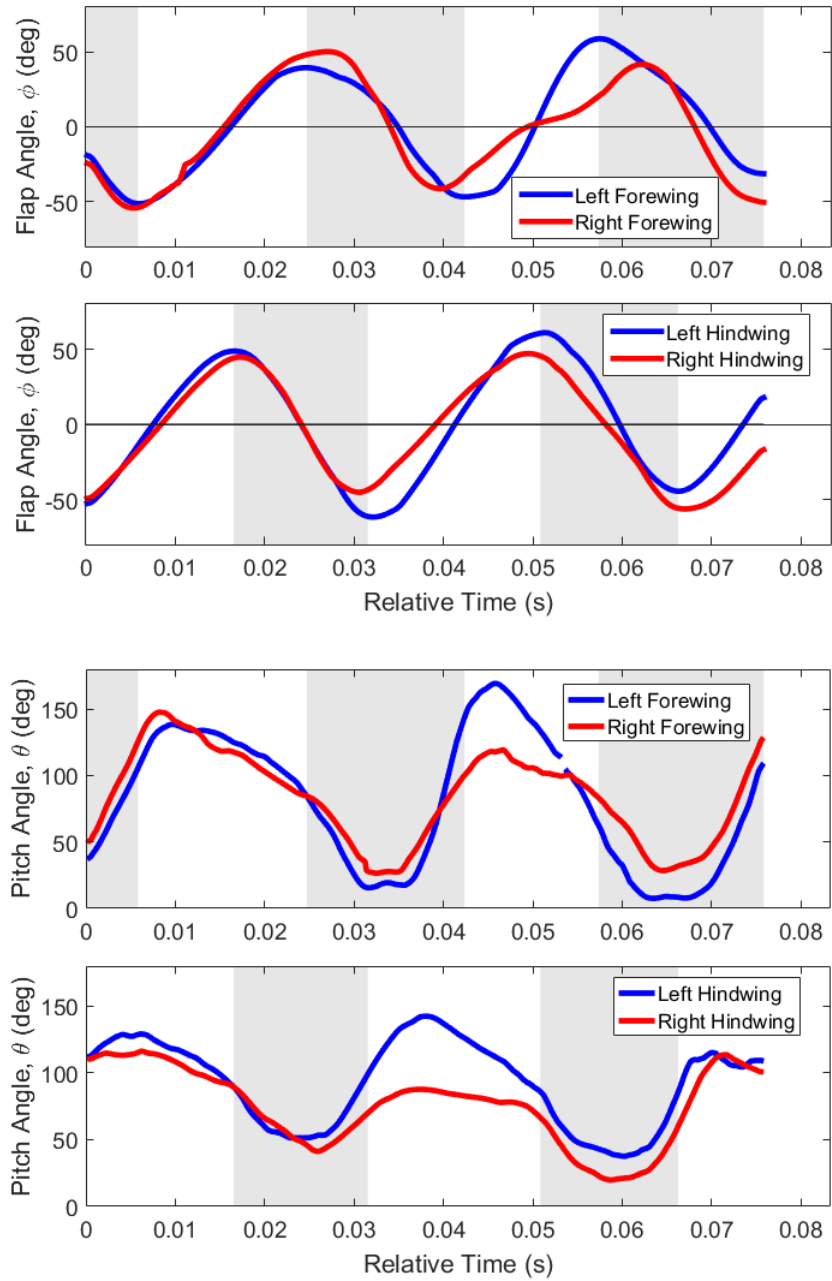
Figure 4.4: Flap and pitch angles for Flight 2. Shaded regions indicate downstrokes.

for free-flying dragonflies were found by Wakeling, who reported values ranging from 64.1° to 115.8° [15].

A primary observation of the given comparison is the asymmetry in downstroke and upstroke durations, as presented in Table 4.3. This can also be readily observed by noting the proportional width of the shaded downstroke sections in Figures 4.3-4.6. The downstroke vs. full wing stroke duration ratio was approximately 45% for all four wings. There was a significant amount of variability in this parameter, with values ranging from 35.6% to 59.4%. All wings experienced instances when the downstroke was longer than the upstroke. Wing stroke frequencies were found to be approximately 30 Hz for both the forewings and the hindwings, but ranged from as low as 24.6 Hz to as high as 34.4 Hz. This is approximately 5 Hz below the standard wingbeat frequency observed for free-flying dragonflies by Ruppell [14], and 9 Hz below the wingbeat frequency found by Wakeling [15].

The progression of the wing pitch angle throughout the flapping cycle was captured with high detail. As expected, the highest rates of change in the pitch angle occurred during stroke reversal for all flights. However, pitch angles were not steady during the translational phase of the stroke, but instead varied throughout. The dragonflies utilized moderately advanced rotation in nearly all cases, completing most of the wing pitching motion before the point of stroke reversal. However, some pitch change always occurred after stroke reversal. Thus, purely advanced rotation was never observed. Symmetrical rotation was found to occur in several cases, such as for both forewings in Flights 1 and 2, and for the right forewing in Flight 3. Moderate delayed rotation was also noted for the hindwings in Flight 1,
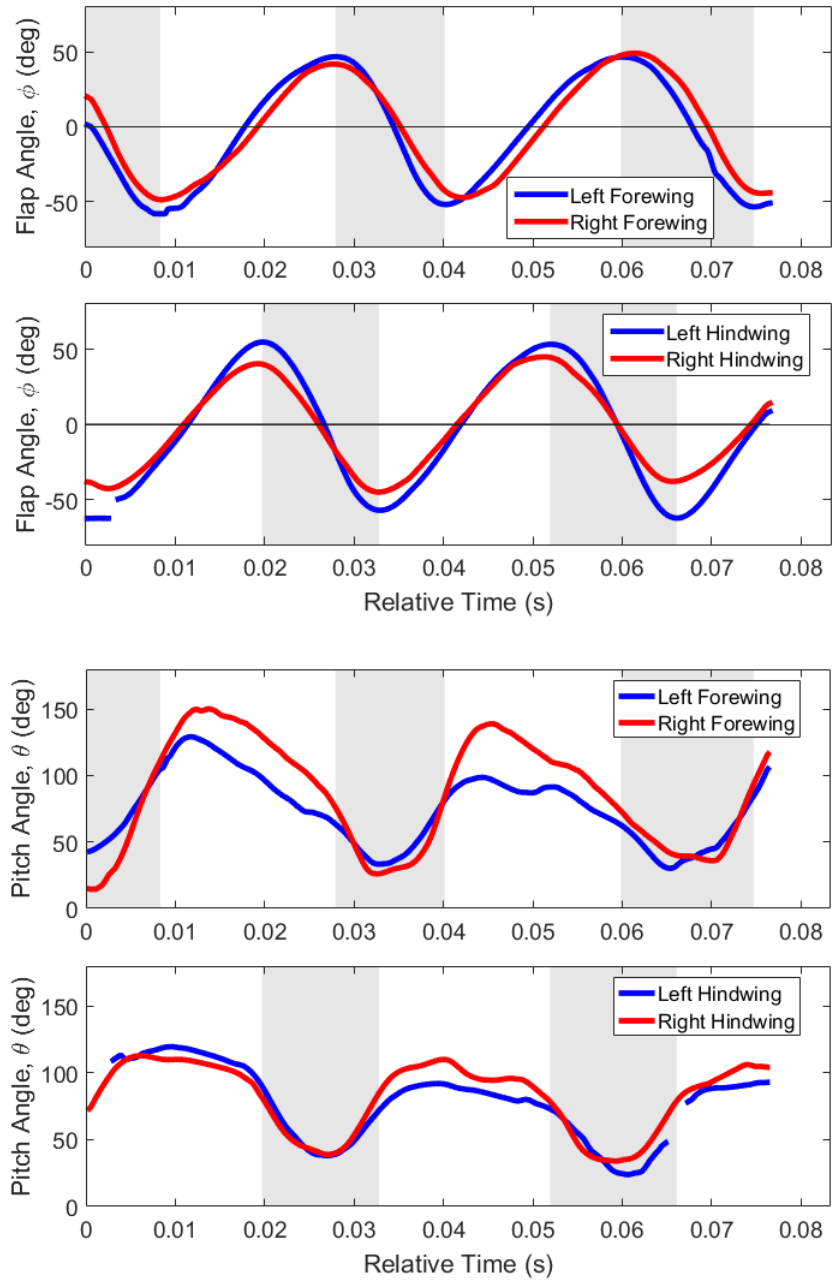
Figure 4.5: Flap and pitch angles for Flight 3. Shaded regions indicate downstrokes.
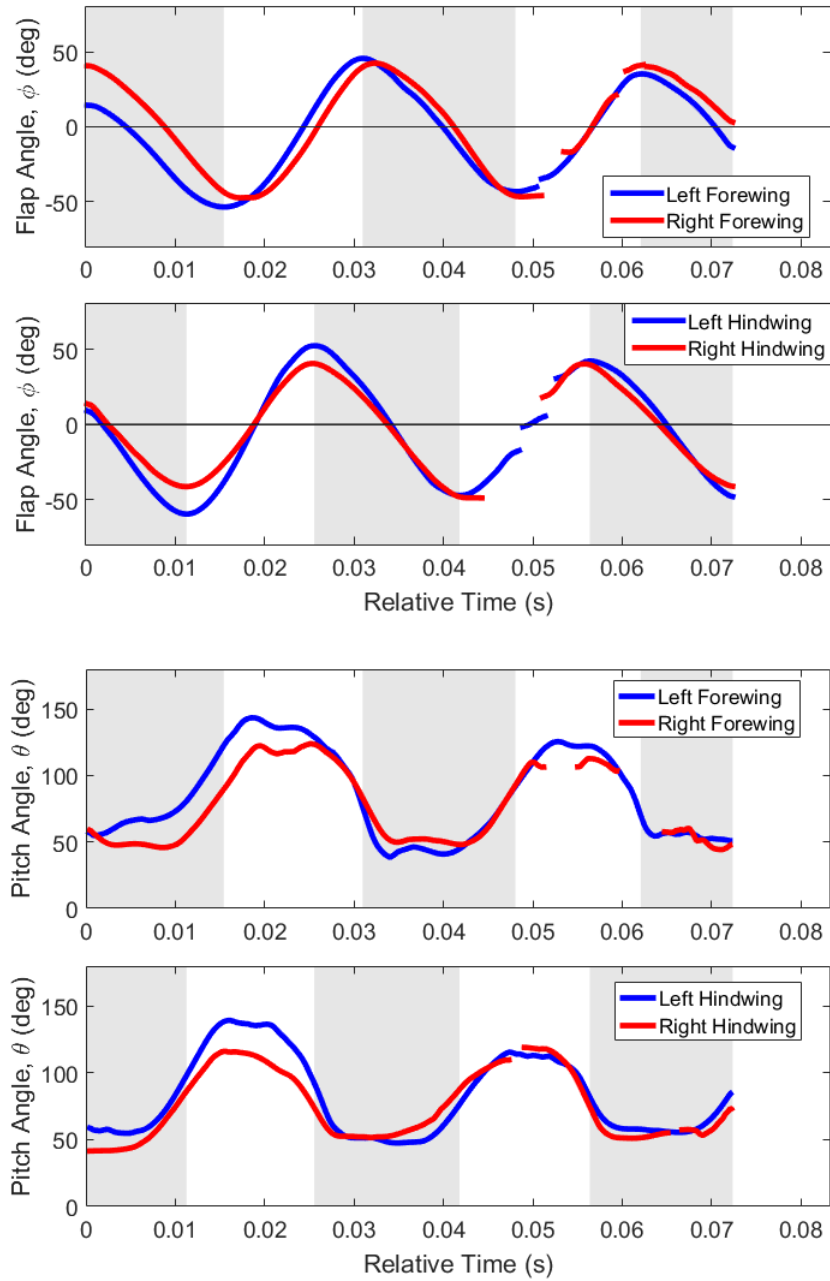
Figure 4.6: Flap and pitch angles for Flight 4. Shaded regions indicate downstrokes.

the right hindwing in Flight 2, and both hindwings in Flight 3 (during pronation only). Thus, it appears that while moderately advanced rotation is standard for unaccelerating Blue Dashers, the phasing of the pitch change is often altered to adjust the aerodynamic forces produced during a wing stroke.

Two types of mid-stroke pitch profiles were observed: a "plateau" profile and a "peak" profile. The plateau-type profile, where the pitch angle was held relatively constant for a significant portion of the translating stroke period, was most common. This was most prominently seen during Flights 1 and 4. The peak-type profile involved higher rates of change in pitch angle during mid-stroke, with a maximum value being held only briefly as the pitching motion reversed direction. Primary examples of this motion are the left forewing and hindwing of Dragonfly 2, and first and second upstrokes of the left and right forewings, respectively, of Dragonfly 3. Some pitch profiles were a combination of the two, with moderate pitching rates throughout the mid-stroke. The pitch angles presented in Li's photogrammetric study of a dragonfly in turning flight exhibit primarily peak-type profiles during the midstroke [16]. However, only three wingbeats were analyzed in that study versus the eight wingbeats presented here, which may explain why the plateau-type pitch angle profiles were not represented.

Statistical data on the variation of the pitch angle θ are cataloged in Table 4.4. The dragonflies exhibited a wide range of peak pitch angles during each half-stroke. Values during the downstroke varied from relatively low angles such as 8° up to conventionally post-stall angles such as 56°. Pitch angles during the upstroke were more aggressive, with a maximum of 169° (only 11° off of the stroke plane)

and a minimum of under 90° in two cases. Although a pitch angle of less than 90° during the upstroke suggests negative lift production, the magnitude of this effect can be lessened when the forward flight velocity of the dragonfly is accounted for. It is possible that the dragonfly used such unusually high values of pitch angle to perform adjustments to its body orientation.

Despite the variability in peak pitch angles, the mean values calculated for the forewings and hindwings were remarkably similar. As shown in Table 4.3, the mean peak value of θ for both forewings was 35° during the downstroke and 135° during the upstroke. For the left and right hindwings, this value was found to be 44° and 40° (respectively) during the downstroke, and 114° and 111° during the upstroke. Thus, we see that the hindwings employed an approximately 10° higher pitch angle during the downstroke and a 20° higher pitch angle during the upstroke. Both wings exhibited more aggressive pitch angles during the upstroke. The mean forewing pitch angle was 10° higher off of the stroke plane during the upstroke than the downstroke, while the mean hindwing pitch angle was about 25° further off of the stroke plane during the upstroke.

Table 4.3: Stroke amplitude and peak pitch angle data for Flights 1-4. Values are presented as mean $\pm$ single standard deviation (minimum value, maximum value).

Wing	Stroke Amp. (Downstroke)	Stroke Amp. (Upstroke)	θ_{min} (Downstroke)	θ_{max} (Upstroke)
Left Forewing	$96\pm8°$	$98\pm9°$	$35\pm16°$	$135\pm19°$
	$(86°, 105°)$	$(79°, 106°)$	$(8°, 55°)$	$(99°, 169°)$
Right Forewing	$95\pm11°$	$100\pm16°$	$35\pm11°$	$135\pm14°$
	$(89°, 120°)$	$(83°, 130°)$	$(14°, 48°)$	$(113°, 150°)$
Left Hindwing	$104\pm8°$	$106\pm11°$	$44\pm10°$	$114\pm19°$
	$(91°, 116°)$	$(90°, 122°)$	$(24°, 56°)$	$(89°, 142°)$
Right Hindwing	$92\pm12°$	$96\pm14°$	$40\pm11°$	$111\pm9°$
	$(82°, 114°)$	$(82°, 120°)$	$(20°, 53°)$	$(88°, 118°)$

71

Table 4.4: Stroke duration and frequency data for Flights 1-4. Values are presented as mean $\pm$ single standard deviation (minimum value, maximum value).

Wing	t_{stroke} (Downstroke)	t_{stroke} (Upstroke)	Wing Stroke Frequency	Downstroke Ratio
L. Forewing	15.1±2.3 ms	18.6±3.5 ms	29.7±2.0 Hz	44.8±7.7%
	(12.2, 17.6 ms)	(14.0, 23.2 ms)	(27.3, 32.1 Hz)	(36.7, 54.9%)
R. Forewing	15.2±1.9 ms	19.3±3.6 ms	29.3±2.7 Hz	44.5±6.7%
	(12.2, 17.8 ms)	(12.6, 22.9 ms)	(24.6, 34.4 Hz)	(35.6, 56.5%)
L. Hindwing	15.2±1.1 ms	18.0±2.7 ms	30.1±2.2 Hz	45.4±4.9%
	(13.1, 16.3 ms)	(14.3, 22.1 ms)	(26.2, 32.7 Hz)	(40.0, 53.2%)
R. Hindwing	15.6±1.8 ms	17.5±3.1 ms	30.8±2.6 Hz	47.4±6.8%
	(13.3, 18.1 ms)	(12.4, 21.8 ms)	(26.6, 34.4 Hz)	(41.0, 59.4%)

4.3 Accelerating Flights

Two straight, accelerating flights were analyzed for comparison to the baseline unaccelerating flight case. Despite the high number of recorded flights, no level accelerating flights were captured. The only significant linear accelerations observed occurred during periods of diving flight. Therefore, as shown in Figure 4.7, both Flights 5 and 6 involve significant diving maneuvers. The abrupt change in dive rate and velocity for Flight 5 corresponds to the dragonfly colliding with the bottom of the test section; however, no kinematic data are presented following this point.
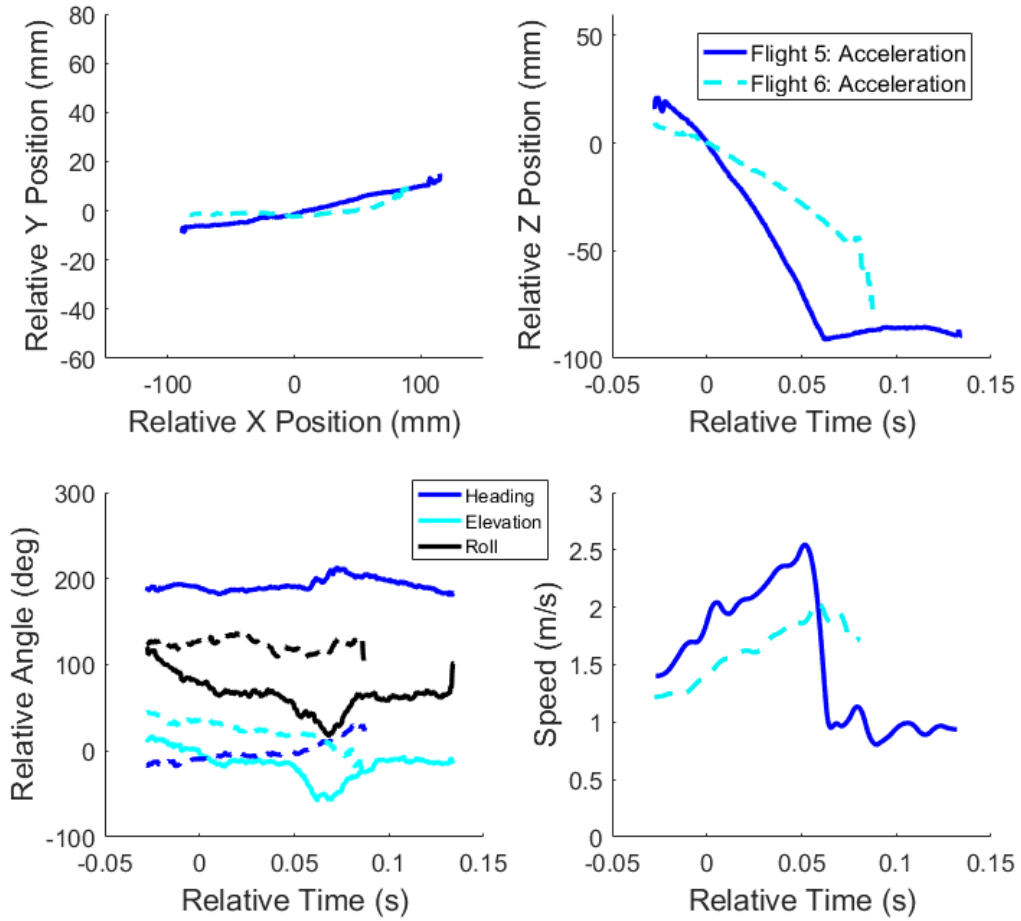
Figure 4.7: Body kinematic data for Flights 5 and 6.

Once again the flapping motion was generally in-phase for the forewings and hindwings individually, but there was phase lag of 80° for the forewings compared to the hindwings as shown by Figures 4.8 and 4.9. Interestingly, the right forewing of dragonfly 6 exhibited faster downstrokes and slower upstrokes than the left forewing, causing the two wings to be in phase for pronation but slightly out of phase during supination. This was not observed for Flight 5. The stroke amplitudes for the diving flights were slightly smaller than for Flights 1-4, particularly for the forewings. One

forewing wing stroke was found to have an amplitude of only 66°, 13° smaller than the shortest wing stroke of the unaccelerating flights.

As with Flights 1-4, the downstrokes were found to be faster than the upstrokes in nearly all cases. The downstroke to full wing stroke ratio was slightly lower for the accelerating flights, and was observed to be only 33.8% for one forewing stroke. Wing stroke frequencies were similar to the unaccelerating flights, averaging approximately 31 Hz. Once again, relatively high amounts of variability were found in this parameter.

The dragonflies primarily employed moderately advanced or symmetrical rotation during the accelerating flights. Both the plateau- and peak-type pitch angle profiles were observed, althought the plateau-type was more common during upstrokes while the peak-type appeared most often during downstrokes. Flight 5 exhibited an unusually small range in pitch angle for the hindwings throughout each wing stroke. The hindwings held a pitch angle of approximately 50° during the downstroke and 100° during the upstroke. This range was generally found to be higher for most tests, although Flight 1 exhibited similarly low amounts of pitch variation for the hindwings. Average values for peak pitch angles reached during the half-strokes were not found to be significantly different between the accelerating and unaccelerating flights, and similar differences in peak forewing and hindwing pitch angles were observed (Table 4.6).
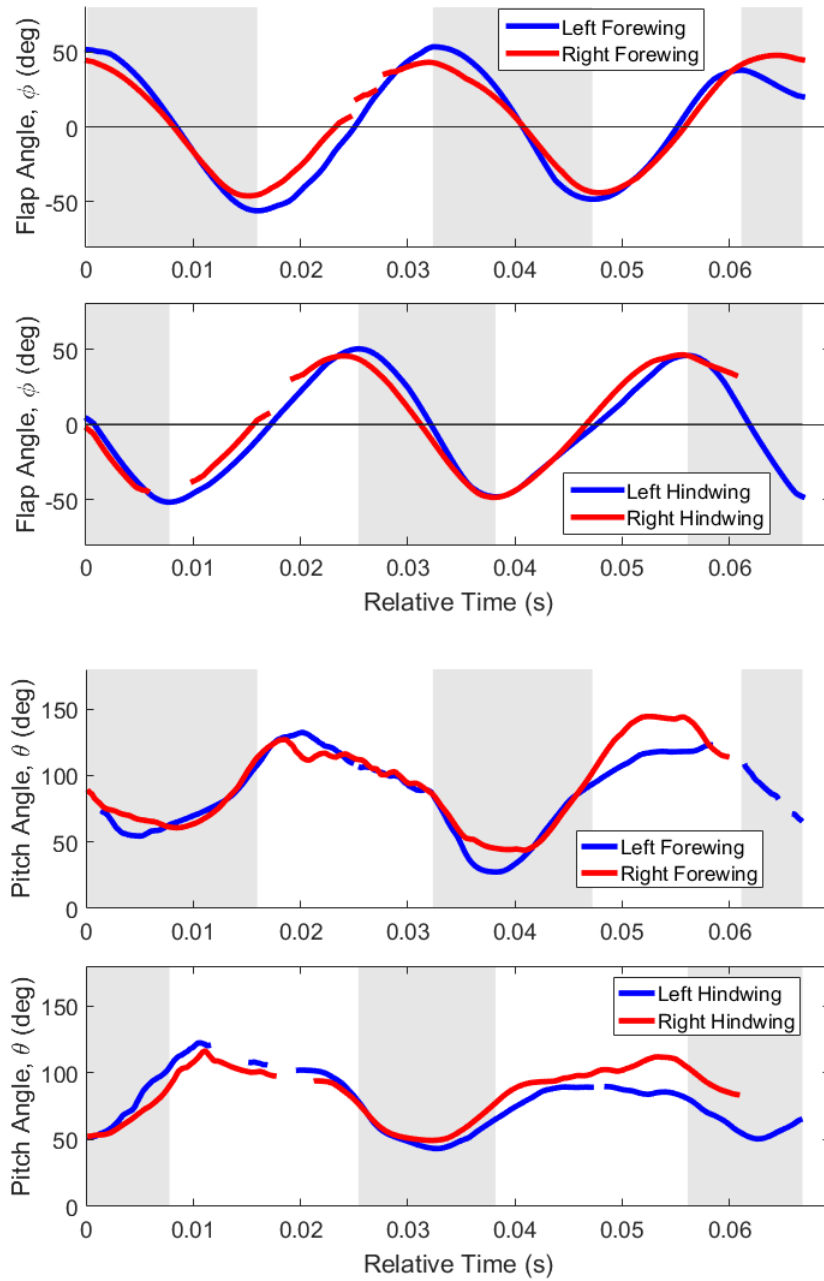
Figure 4.8: Flap and pitch angles for Flight 5. Shaded regions indicate downstrokes.
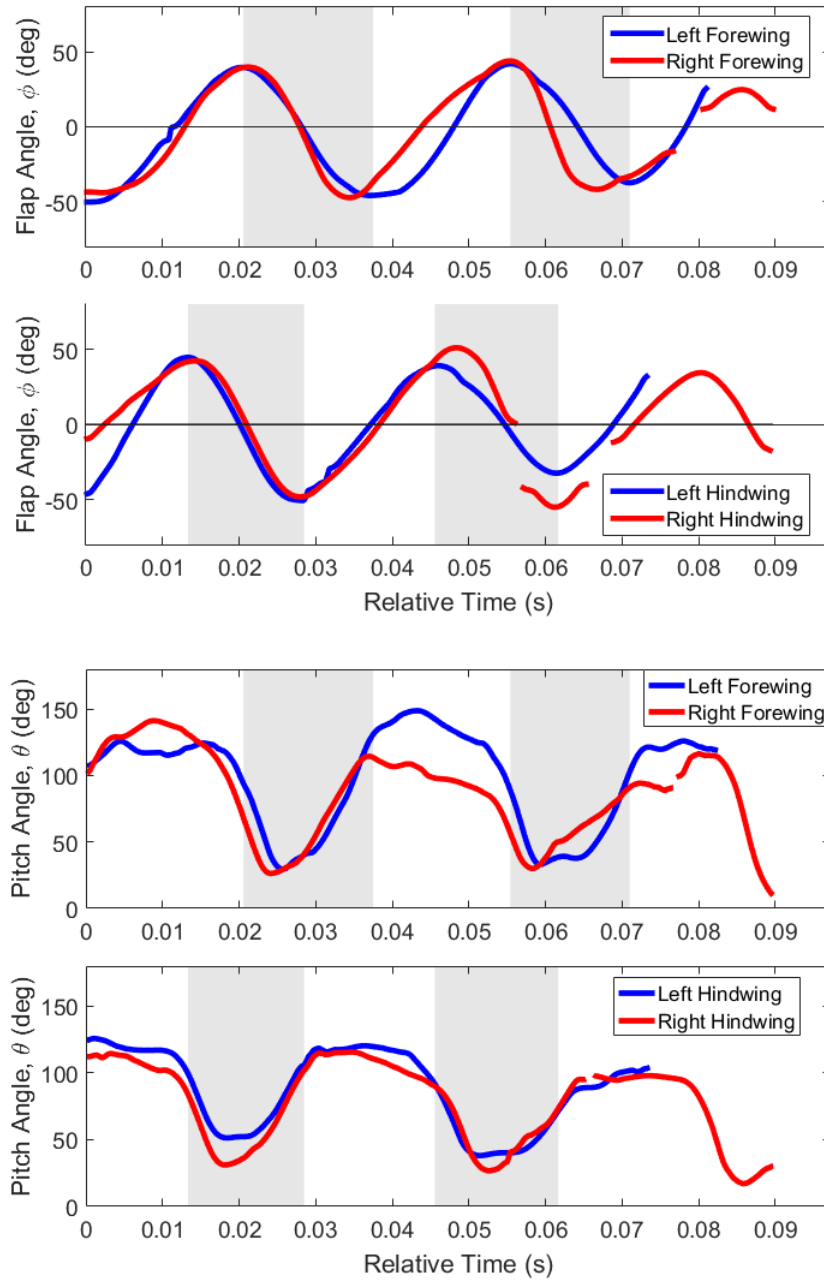
Figure 4.9: Flap and pitch angles for Flight 6. Shaded regions indicate downstrokes.

76

Table 4.5: Stroke amplitude and peak pitch angle data for Flights 5-6. Values are presented as mean ± single standard deviation (minimum value, maximum value).

Wing	Stroke Amp. (Downstroke)	Stroke Amp. (Upstroke)	θ_{min} (Downstroke)	θ_{max} (Upstroke)
Left Forewing	94±13°	94±11°	36±12°	131±10°
	(80°, 108°)	(86°, 110°)	(27°, 54°)	(123°, 149°)
Right Forewing	88±2°	85±11°	40±16°	129±14°
	(86°, 90°)	(66°, 92°)	(26°, 61°)	(114°, 144°)
Left Hindwing	90±12°	95±6°	46±6°	112±16°
	(71°, 98°)	(90°, 102°)	(38°, 51°)	(89°, 126°)
Right Hindwing	97±8°	93±5°	31±14°	111±8°
	(90°, 106°)	(89°, 99°)	(17°, 49°)	(98°, 117°)

Table 4.6: Stroke duration and frequency data for Flights 5-6. Values are presented as mean ± single standard deviation (minimum value, maximum value).

Wing	t_{stroke} (Downstroke)	t_{stroke} (Upstroke)	Wing Stroke Frequency	Downstroke Ratio
L. Forewing	15.8±0.9 ms	17.2±2.7 ms	30.5±2.8 Hz	48.1±2.2%
	(14.9, 16.9 ms)	(13.9, 20.4 ms)	(26.8, 34.8 Hz)	(45.4, 51.7%)
R. Forewing	13.8±2.3 ms	18.5±1.9 ms	31.1±1.2 Hz	42.1±6.5%
	(10.7, 16.0 ms)	(16.5, 21.0 ms)	(29.1, 33.2 Hz)	(33.8, 49.1%)
L. Hindwing	13.7±2.4 ms	17.5±0.4 ms	32.3±1.9 Hz	43.3±4.5%
	(10.7, 16.1 ms)	(17.1, 17.9 ms)	(30.1, 35.0 Hz)	(37.4, 48.5%)
R. Hindwing	13.5±0.7 ms	19.0±1.2 ms	30.6±0.9 Hz	41.1±2.5%
	(12.6, 14.0 ms)	(17.6, 20.4 ms)	(29.3, 31.6 Hz)	(38.2, 44.3%)

4.4 Climbing Flights

Flights 7 and 8 consist of straight, constant-speed, steady climbs. These flights were selected due to their turn-free nature and close alignment in climb rate. It should be noted that dragonfly 7 weighed 79% more than dragonfly 8, which may correspond to differences in wing kinematics. As shown in Figure 4.10, all body angles except roll are similar for the two specimens, and the dragonfly yaw angles are small. The climb rates are approximately 0.6 m/s for both dragonflies, but the mean flight speed of dragonfly 8 is approximately 80% higher than the mean speed
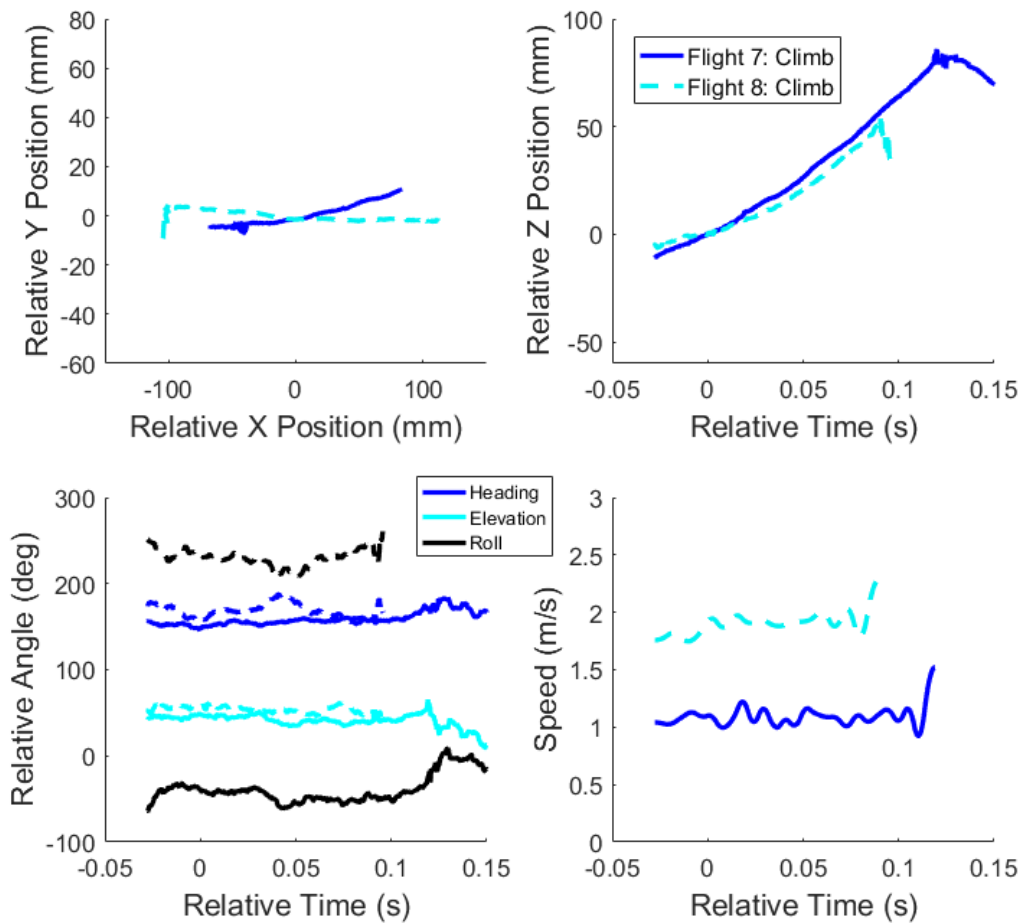
Figure 4.10: Body kinematic data for Flights 7 and 8.

of dragonfly 7.

Figures 4.11 and 4.12 show the wing flap and pitch angles for the two climbing flights. Out-of-phase stroking is observed for both flights, with an average phase difference of 79°. Once again, the forewing and hindwing pairs are each individually in phase with each other in terms of both flapping and pitching motion. As shown in Table 4.7, the stroke amplitude values are not greatly different from those found in Flights 1-6. However, the right forewing and hindwing were found to have ap-

proximately 10° higher stroke amplitudes. Since the dragonflies were not turning, this could correspond to an adjustment in roll angle or another trimming maneuver. Wing stroke frequencies were marginally higher for the climbing flights, averaging approximately 32 Hz. The greatest change was found in the downstroke ratio, which was higher than usual for the left wings. Notably, the left forewing was found to generally have a longer downstroke than upstroke.

A key difference observed between the climbing and unaccelerating flights is that the dragonflies in Flights 7 and 8 exclusively employed advanced rotation for the forewings, while generally using symmetrical rotation for the hindwings. The advanced rotation of the forewings did not entirely take place before stroke reversal, but was noticeably more aggressive than the advanced rotation observed for the unaccelerating flights. As with Flights 1-4, both plateau- and peak-type pitch angle profiles were present, but plateau profiles were generally favored. The clearest examples of peak-type pitch profiles occurred during the downstrokes. Peak pitch values were considerably less aggressive than usual for all four wings for Flights 7 and 8. Minimum pitch angles were approximately 10° lower during the downstroke, and maximum pitch angles were approximately 5° higher during the upstroke. The right forewing was not included in this trend during the upstroke, and exhibited an unusually low peak pitch value of 118°. This could be related to the trimming maneuvers hypothesized to be responsible for the right-side stroke amplitude increases.
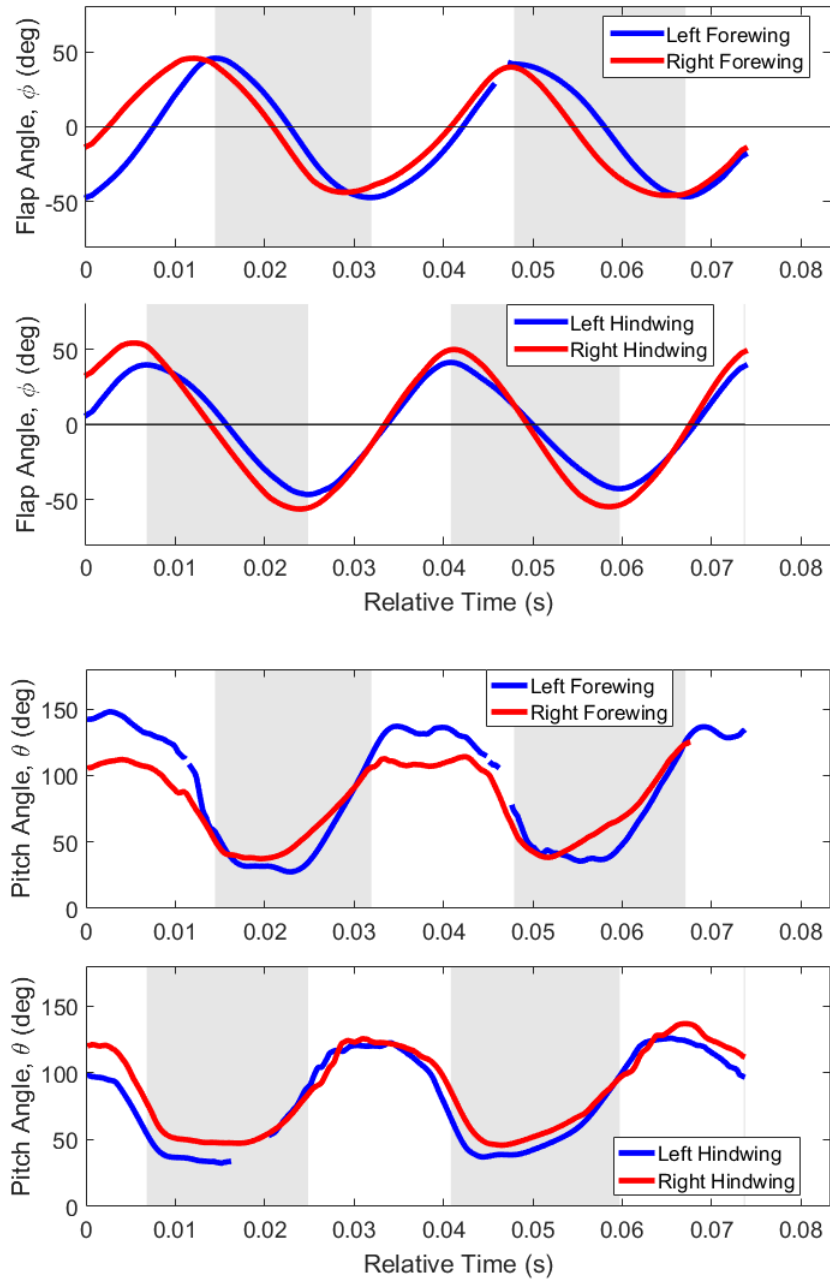
Figure 4.11: Flap and pitch angles for Flight 7. Shaded regions indicate downstrokes.
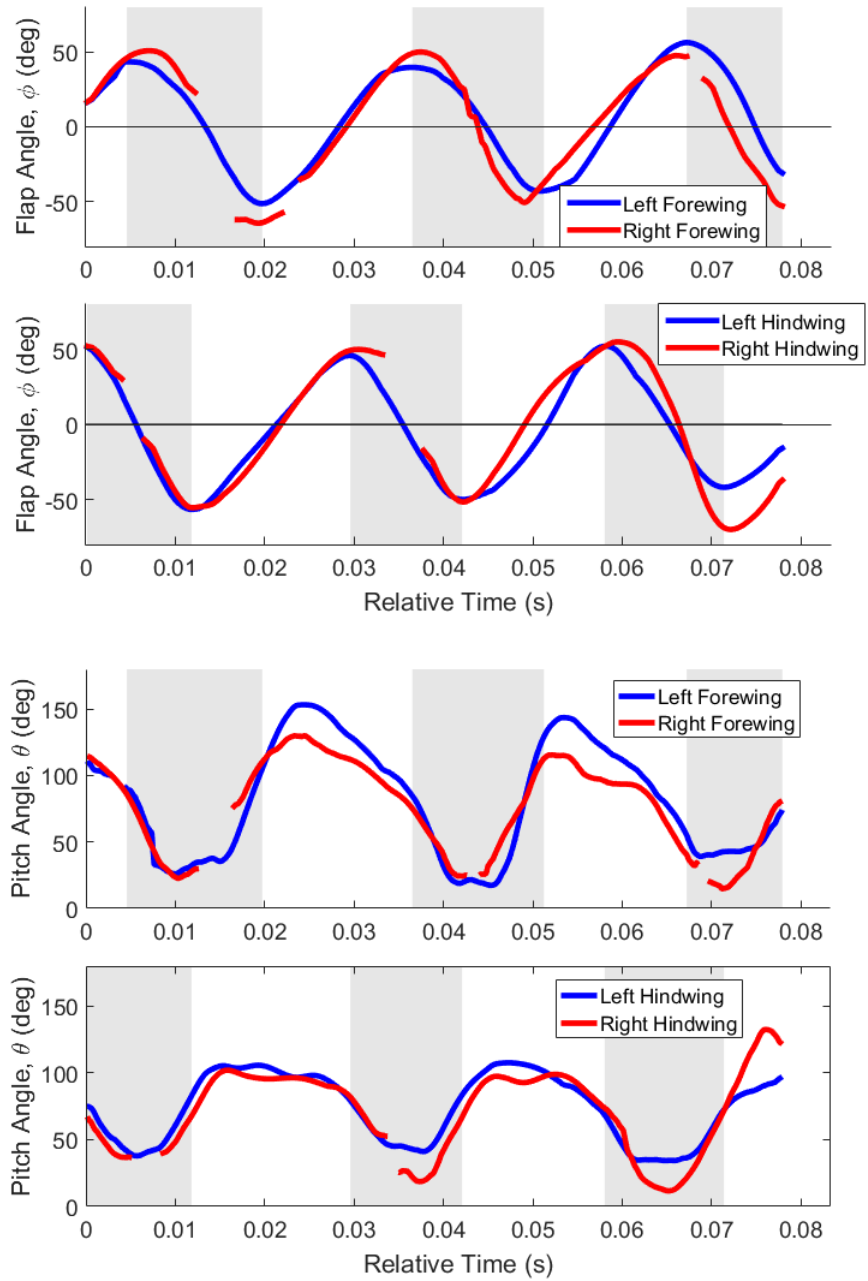
Figure 4.12: Flap and pitch angles for Flight 8. Shaded regions indicate downstrokes.

Table 4.7: Stroke amplitude and peak pitch angle data for Flights 7-8. Values are presented as mean $\pm$ single standard deviation (minimum value, maximum value).

Wing	Stroke Amp. (Downstroke)	Stroke Amp. (Upstroke)	θ_{min} (Downstroke)	θ_{max} (Upstroke)
Left Forewing	$90\pm5°$	$93\pm4°$	$29\pm9°$	$144\pm7°$
	$(83°, 95°)$	$(89°, 99°)$	$(17°, 39°)$	$(137°, 153°)$
Right Forewing	$98\pm12°$	$99\pm15°$	$27\pm10°$	$118\pm8°$
	$(86°, 115°)$	$(84°, 114°)$	$(15°, 38°)$	$(112°, 130°)$
Left Hindwing	$94\pm9°$	$93\pm11°$	$36\pm4°$	$116\pm10°$
	$(84°, 108°)$	$(81°, 102°)$	$(32°, 41°)$	$(106°, 126°)$
Right Hindwing	$109\pm9°$	$107\pm3°$	$32\pm16°$	$120\pm16°$
	$(102°, 125°)$	$(105°, 110°)$	$(12°, 47°)$	$(99°, 137°)$

Table 4.8: Stroke duration and frequency data for Flights 7-8. Values are presented as mean ± single standard deviation (minimum value, maximum value).

Wing	t_{stroke} (Downstroke)	t_{stroke} (Upstroke)	Wing Stroke Frequency	Downstroke Ratio
L. Forewing	16.6±2.1 ms	15.8±1.0 ms	30.9±1.5 Hz	50.7±3.8%
	(14.7, 19.2 ms)	(14.3, 16.8 ms)	(28.5, 32.6 Hz)	(46.7, 55.0%)
R. Forewing	14.0±2.9 ms	18.0±0.8 ms	31.9±3.2 Hz	42.7±4.2%
	(11.7, 17.5 ms)	(17.1, 18.6 ms)	(27.7, 34.8 Hz)	(38.9, 48.5%)
L. Hindwing	14.9±3.3 ms	15.9±1.6 ms	32.1±2.6 Hz	47.9±7.0%
	(11.7, 18.9 ms)	(13.9, 17.8 ms)	(28.7, 35.1 Hz)	(39.6, 57.6%)
R. Hindwing	13.7±2.3 ms	18.0±0.7 ms	31.6±2.5 Hz	43.6±4.3%
	(11.8, 17.1 ms)	(17.2, 18.6 ms)	(28.0, 34.4 Hz)	(39.0, 49.4%)

4.5   Turning Flights

Two turning flights were analyzed to investigate asymmetries between the left and right wing pairs during radial accelerations. Flight 9 consists of 2.5 wing strokes, while Flight 10 is much shorter at just under 1.5 wing strokes due to poor wing visibility. Very few level turns were captured during testing, thus limiting the quality of the videos that could be analyzed. As can be seen in Figure 4.13, the radius of curvature of both turns is approximately equal. Dragonfly 9 is turning left while Dragonfly 10 is turning right. Flight 9 is relatively level, but the turn in Flight
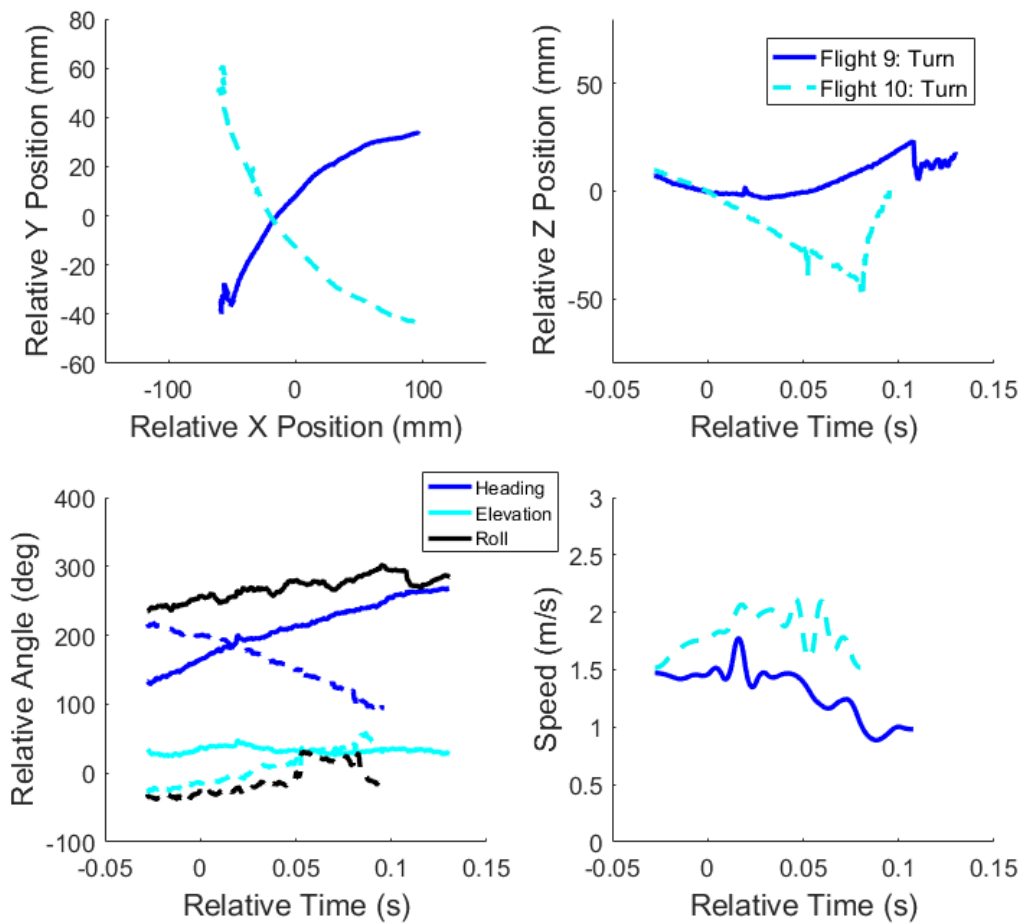
Figure 4.13: Body kinematic data for Flights 9 and 10.

10 includes a moderate dive. Both dragonflies were observed to perform primarily pitching, rather than yawing, turns.

As shown in Figures 4.14 and 4.15, the forewings and hindwings are once again found to be out of phase, with the hindwings leading the forewings. The average phase difference between the forewings and hindwings was 74°, although the phase difference in Flight 9 was only 61°, the lowest of all 12 flights. Tables 4.9 and 4.10 catalog the wing kinematic data organized by the inside and outside wings with

respect to the turn direction. The stroke amplitudes of the inside forewings were found to be 5-10° larger than those of the outside forewings. This was not found to hold true for the hindwings. The stroke amplitudes of all four wings were observed to be smaller than those found in Flights 1-4. The hindwings had a stroke amplitude 10-20° smaller than seen for the straight flights, while the forewing stroke amplitudes were 20-30° smaller for the turning flights. In one instance, the outside forewing had a half-stroke with an amplitude of only 58°.

The wing stroke frequencies were found to be about 15% higher for the turning flights than the straight flights, averaging approximately 35 Hz and reaching values as high as 36.9 Hz. In fact, three of the four wings had minimum wing stroke frequency values that were higher than the maximum frequency values for the corresponding wings in Flights 1-4. A unique quality of the turning flights was that three of the four wings exhibited downstrokes that were longer in duration than the upstrokes; this was the only set of flights where this was observed. The inside forewing and hindwing exhibited higher downstroke ratios than the outside wings.

Moderately advanced or symmetric rotation was used in nearly all wing strokes, although the right hindwing of dragonfly 9 showed nearly fully delayed rotation. In this flight, the dragonfly was turning left, so the use of delayed rotation on the right side is surprising as it would be expected to cause a reduction in aerodynamic force. However, this rotation occurs near the end of the sequence where marker data were most sparse, so it is possible that the phasing of the rotation was not characterized accurately.

The dragonflies in Flights 9 and 10 generally exhibited much higher peak pitch
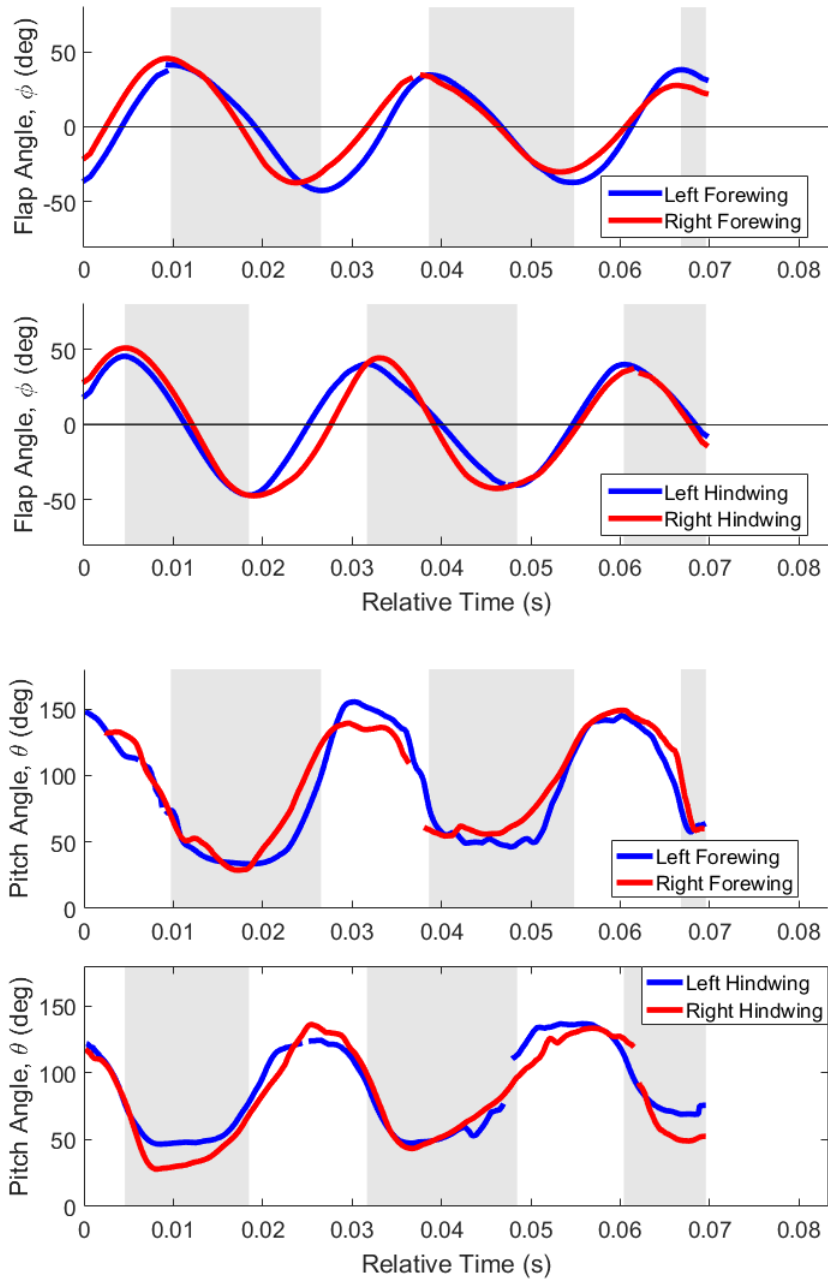
Figure 4.14: Flap and pitch angles for Flight 9. Shaded regions indicate downstrokes.
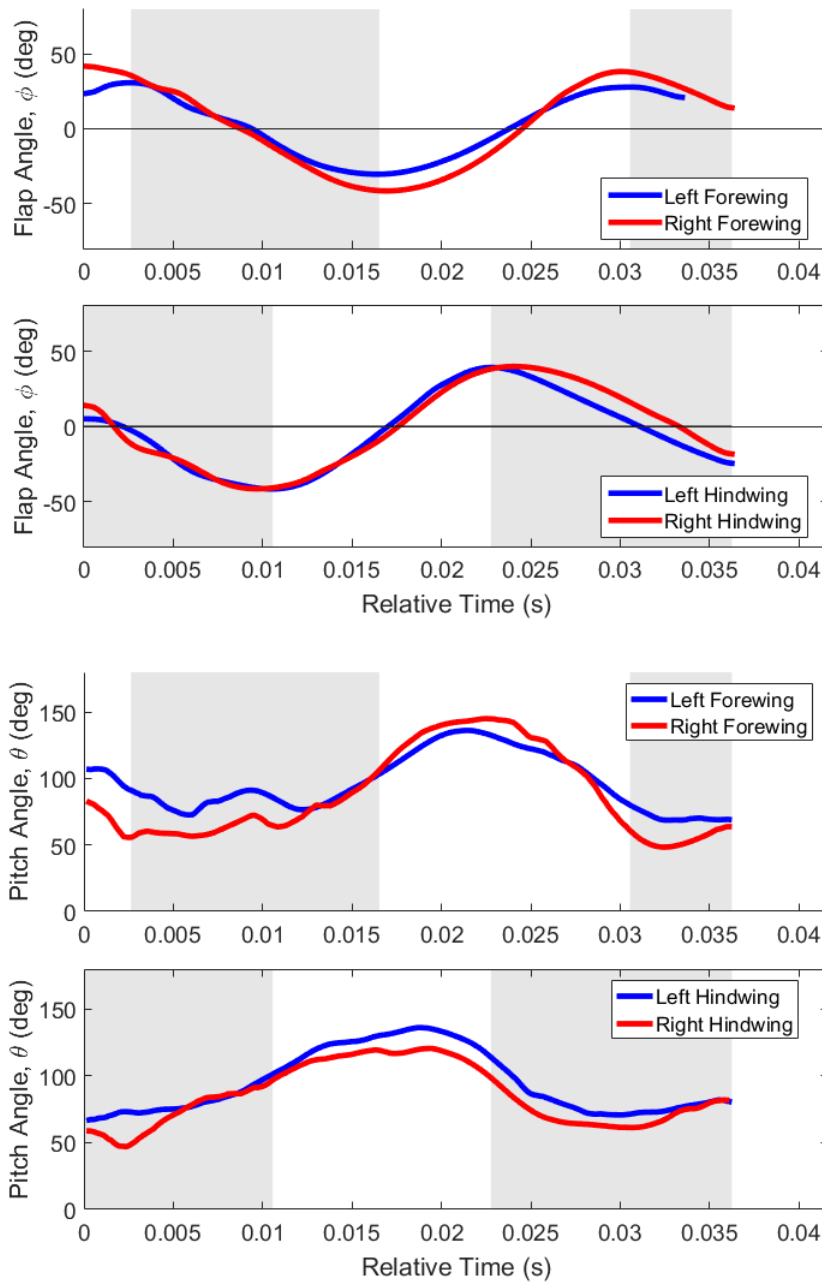
Figure 4.15: Flap and pitch angles for Flight 10. Shaded regions indicate down-strokes.

angle values than those in Flights 1-4, as shown in Table 4.9. Forewing peak pitch angle values were 10-20° higher during the downstroke and 5-10° higher (representing a less aggressive pitch angle) during the upstroke. Hindwing peak pitch values were approximately 10° higher during the downstroke and 15-20° higher during the upstroke.

Table 4.9: Stroke amplitude and peak pitch angle data for Flights 9-10. Values are presented as mean ± single standard deviation (minimum value, maximum value).

Wing	Stroke Amp. (Downstroke)	Stroke Amp. (Upstroke)	θ_{min} (Downstroke)	θ_{max} (Upstroke)
Inside	80±7°	78±2°	48±9°	148±6°
Forewing	(72°, 84°)	(75°, 80°)	(34°, 57°)	(145°, 155°)
Outside	74±13°	64±7°	56±20°	139±7°
Forewing	(65°, 83°)	(58°, 72°)	(29°, 73°)	(133°, 149°)
Inside	85±7°	84±5°	54±10°	127±9°
Hindwing	(81°, 92°)	(80°, 87°)	(47°, 69°)	(121°, 137°)
Outside	93±8°	84±7°	48±18°	135±2°
Hindwing	(87°, 98°)	(79°, 92°)	(28°, 71°)	(133°, 136°)

Table 4.10: Stroke duration and frequency data for Flights 9-10. Values are presented as mean ± single standard deviation (minimum value, maximum value).

Wing	t_{stroke} (Downstroke)	t_{stroke} (Upstroke)	Wing Stroke Frequency	Downstroke Ratio
Inside FW	16.6±0.3 ms	12.4±0.7 ms	34.7±1.0 Hz	57.3±0.9%
	(16.3, 16.8 ms)	(11.9, 13.2 ms)	(33.3, 35.5 Hz)	(56.0, 58.2%)
Outside FW	14.9±0.7 ms	13.7±0.7 ms	35.0±0.9 Hz	52.3±2.0%
	(14.4, 15.4 ms)	(12.9, 14.2 ms)	(33.8, 35.8 Hz)	(50.5, 54.4%)
Inside HW	15.0±1.6 ms	12.6±0.9 ms	35.0±1.8 Hz	55.3±3.6%
	(13.9, 16.8 ms)	(11.9, 13.2 ms)	(33.3, 36.9 Hz)	(51.3, 58.5%)
Outside HW	13.8±0.8 ms	13.8±1.4 ms	35.8±0.8 Hz	48.6±1.8%
	(13.2, 14.3 ms)	(12.2, 15.0 ms)	(35.3, 36.7 Hz)	(46.8, 50.5%)

4.6   Species Comparison

In order to investigate any significant differences in kinematics between various dragonfly species, straight and unaccelerating flights of a Common Pondhawk (Flight 11) and a Spot-Winged Glider (Flight 12) were analyzed for comparison with the data presented in Section 4.2. Common Pondhawks are approximately equal in size to Blue Dashers, and exhibit similar "percher" flight behavior. Spot-Winged Gliders, on the other hand, are slightly larger (body mass 200 mg) and are highly migratory in nature. Spot-Winged Gliders are relatives of the Globe Skimmer, and

have been known to migrate over hundreds of miles. Thus, the objective of this comparison was to investigate the presence of kinematic differences between dragonflies of both similar and different sizes and flight behaviors. It should be noted that because only one flight was analyzed for each species of dragonfly, kinematic differences must be major to be considered statistically significant.

As illustrated in Figure 4.16, the vertical position, orientation angle, and velocity data for these two flights are remarkably similar. Flight 12 does include a mild turn that precedes the straight section, but this period is omitted in the kinematic analysis. As shown in Figure 4.17, the availability of wing kinematic data is intermittent throughout Flight 11 due to visibility problems for certain wings, as well as a section of the test where the roll angle was not determined accurately. Nevertheless, most kinematic parameters were still able to be found for this test.

Both the Common Pondhawk and the Spot-Winged Glider were observed to flap highly out of phase, with the Common Pondhawk exhibiting 88° of phase difference and the Spot-Winged Glider employing 96° of phase difference. The Spot-Winged Glider exhibited a mild version of the two-step flap profile observed in Flights 1 and 2. Downstroke ratios for both the Common Pondhawk and the Spot-Winged Glider were approximately 45% for all four wings (see tables 4.11 and 4.13), similar to that of the Blue Dasher in unaccelerating flight. The Common Pondhawk utilized wing stroke frequencies between 32.2 and 34.1 Hz, which were approximately 10% higher than those of the Blue Dasher. Meanwhile, the Spot-Winged Glider flapped its wings much more slowly, with a mean wing stroke frequency of 24.5 Hz and a lower limit of 22 Hz. This is much lower than any wingbeat fre-
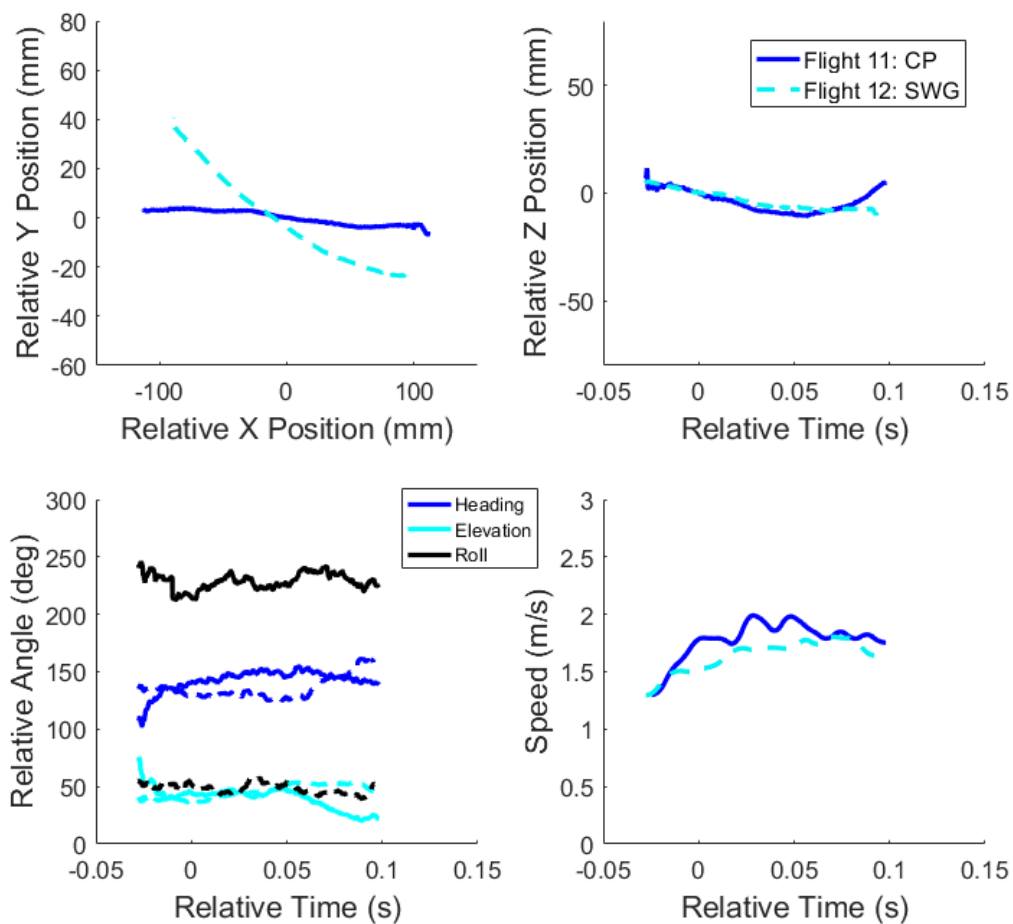
Figure 4.16: Body kinematic data for Flights 11 and 12.

quencies observed by Ruppell in his 1989 study of free-flying dragonfly species: the lowest frequencies he observed were 29 Hz for large (600 mg) dragonflies.

Wingbeat angle, duration, and frequency data were calculated collectively for both forewings and hindwings for each flight, since insufficient data were present to perform statistical analysis for each wing individually. Table 4.12 shows that the Common Pondhawk utilized 10-20° smaller amplitudes for its forewings than the Blue Dasher in Flights 1-4, but approximately equal stroke amplitudes for its
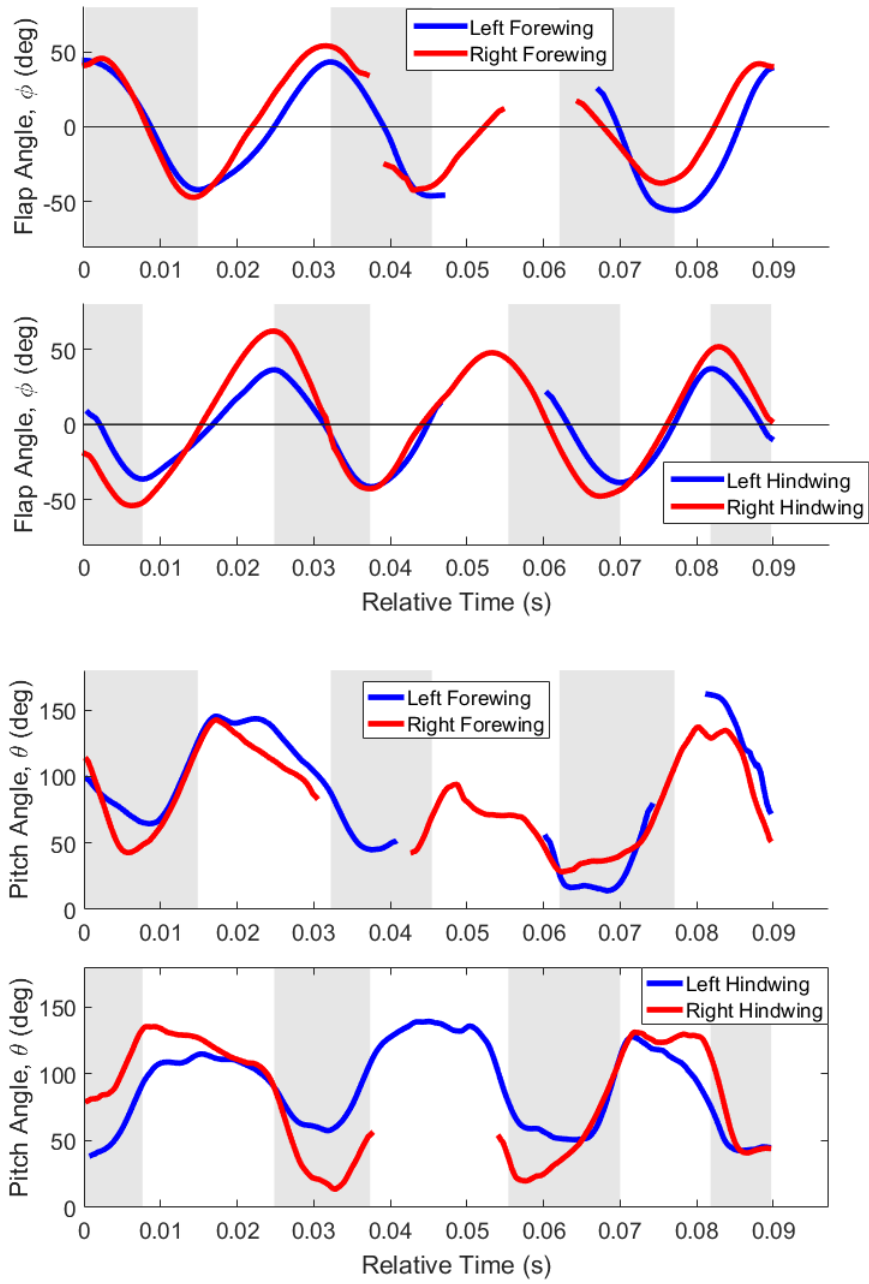
Figure 4.17: Flap and pitch angles for Flight 11. Shaded regions indicate down-strokes.

93
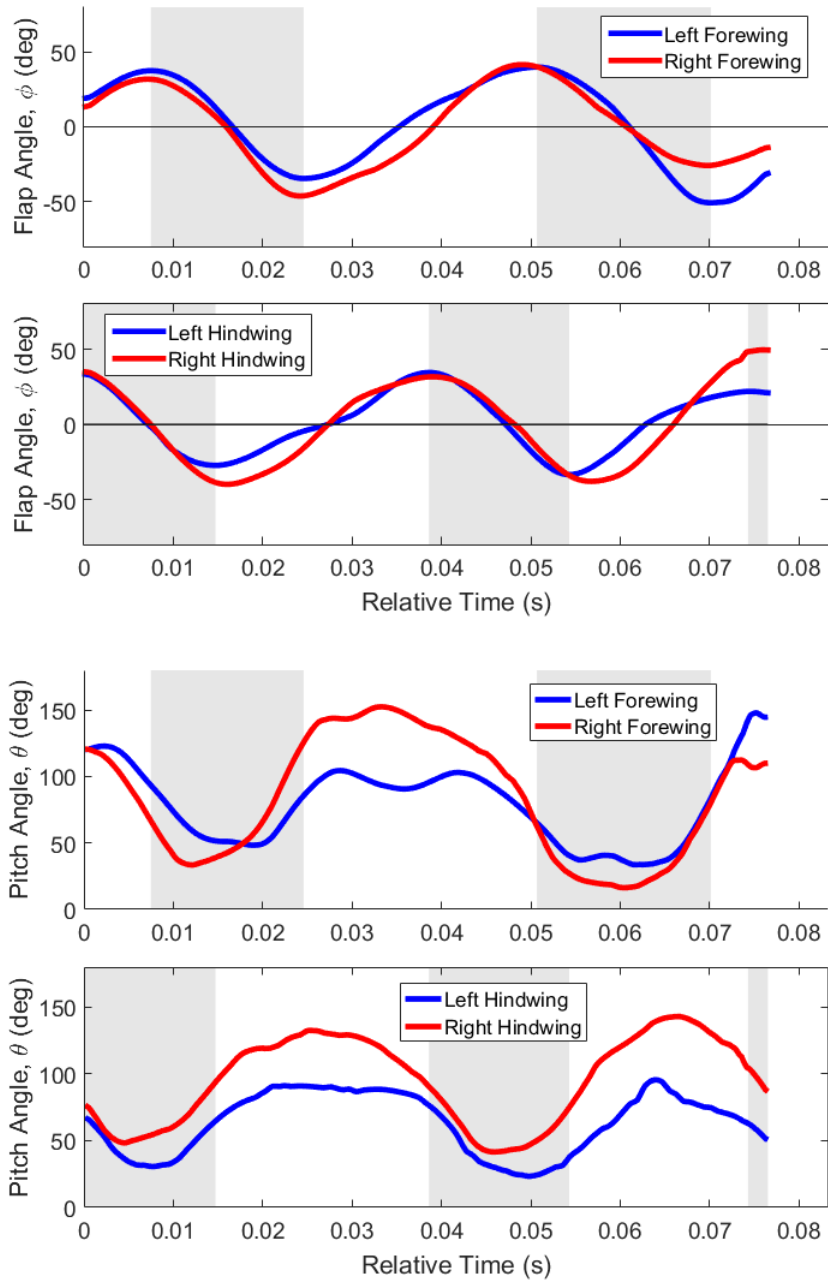
Figure 4.18: Flap and pitch angles for Flight 12. Shaded regions indicate down-strokes.

hindwings. On the other hand, the data for Flight 12 (Table 4.14) show that the Spot-Winged Glider used significantly shorter strokes for all four of its wings than both the Common Pondhawk and the Blue Dasher. The right forewing of the Spot-Winged Glider in particular saw very small stroke amplitudes; its amplitude of 55° during the third half-stroke was the smallest stroke amplitude observed across all 12 tests. The stroke amplitude values for the left forewing were slightly larger for half-strokes 1 and 2, but 36° greater for half-stroke 3.

As seen in Figure 4.17, the Common Pondhawk primarily utilized highly advanced rotation, and did not favor symmetrical rotation around the stroke reversal point like the Blue Dasher. The Spot-Winged Glider, on the other hand, utilized rotation that was almost fully symmetrical (Figure 4.18). The Common Pondhawk exhibited both plateau-type and peak-type pitch angle profiles, while the Spot-Winged Glider tended to hold its pitch angle fairly steady throughout the translational period of the wing stroke. The Common Pondhawk reached peak forewing pitch angles that were comparable to those from Flights 1-4, but its hindwings held slightly higher maximum pitch values during the upstroke and slightly lower minimum values during the downstroke. The Spot-Winged Glider exhibited similar peak wing pitch angles to the unaccelerating Blue Dashers, but its right forewing and hindwing held much higher pitch angles during their respective upstrokes than the wings on the left side of the dragonfly. It is possible that the higher pitch angles were used to compensate for the shorter stroke amplitudes of the right wings, although it is not known why the dragonfly chose to flap its wings asymmetrically.

Table 4.11: Stroke duration and frequency data for Flight 11. Values are presented as mean $\pm$ single standard deviation (minimum value, maximum value). Standard deviation values are omitted if insufficient data are available.

Wing	t_{stroke} (Downstroke)	t_{stroke} (Upstroke)	Wing Stroke Frequency	Downstroke Ratio
Forewings	15.7 ms	15.5$\pm$2.7 ms	33.6$\pm$2.1 Hz	50.6$\pm$7.1%
	(12.5, 18.5 ms)	(12.4, 18.1 ms)	(30.6, 37.9 Hz)	(40.9, 59.9%)
Hindwings	12.8$\pm$1.5 ms	17.4 ms	33.3$\pm$1.8 Hz	44.4$\pm$4.5%
	(11.3, 14.7 ms)	(17.4, 17.4 ms)	(30.9, 36.0 Hz)	(39.1, 53.5%)

Table 4.12: Stroke amplitude and peak pitch angle data for Flight 11. Values are presented as mean $\pm$ single standard deviation (minimum value, maximum value). Standard deviation values are omitted if insufficient data are available.

Wings	Stroke Amp. (Downstroke)	Stroke Amp. (Upstroke)	θ_{min} (Downstroke)	θ_{max} (Upstroke)
Forewings	95°	91°	38$\pm$17°	130$\pm$9°
	(78°, 116°)	(73°, 105°)	(15°, 58°)	(115°, 139°)
Hindwings	91$\pm$4°	93°	39$\pm$19°	136$\pm$25°
	(87°, 97°)	(85°, 101°)	(14°, 65°)	(94°, 162°)

Table 4.13: Stroke duration and frequency data for Flight 12. Values are presented as mean $\pm$ single standard deviation (minimum value, maximum value). Standard deviation values are omitted if insufficient data are available.

Wing	t_{stroke} (Downstroke)	t_{stroke} (Upstroke)	Wing Stroke Frequency	Downstroke Ratio
Forewings	16.8$\pm$1.8 ms	21.2$\pm$2.4 ms	26.1$\pm$1.5 Hz	44.2$\pm$4.2%
	(15.7, 18.9 ms)	(18.5, 23.9 ms)	(24.2, 28.0 Hz)	(39.6, 50.6%)
Hindwings	18.6 ms	25.5 ms	22.7$\pm$0.9 Hz	42.1$\pm$2.6%
	(17.1, 20.7 ms)	(24.9, 26.1 ms)	(22.0, 23.8 Hz)	(39.5, 45.4%)

Table 4.14: Stroke amplitude and peak pitch angle data for Flight 12. Values are presented as mean $\pm$ single standard deviation (minimum value, maximum value). Standard deviation values are omitted if insufficient data are available.

Wings	Stroke Amp. (Downstroke)	Stroke Amp. (Upstroke)	θ_{min} (Downstroke)	θ_{max} (Upstroke)
Forewings	71°	69$\pm$14°	36$\pm$11°	116$\pm$26°
	(68°, 75°)	(55°, 87°)	(23°, 48°)	(91°, 143°)
Hindwings	77$\pm$10°	81°	33$\pm$13°	127$\pm$20°
	(67°, 91°)	(75°, 88°)	(16°, 48°)	(103°, 152°)

Chapter 5: Conclusions

5.1 Overview

The work presented in this thesis serves as a first look into the tandem-wing kinematic data collected for free-flying dragonflies in a custom-made experimental system. The unique experimental setup, iteratively designed over the course of twelve months, proved to be successful and video data of nearly 700 individual tests were collected. Basic kinematic data were presented for twelve individual flights. Blue Dashers undergoing unaccelerating flight, accelerating flight, climbing flight, and turning flight were studied, and one flight each of a Common Pondhawk and a Spot-Winged Glider were compared to investigate kinematic differences between dragonfly species.

5.2 Conclusions of the Study

1. Perhaps the most significant conclusion of the present study is that dragonflies exhibit an enormous amount of variation in their wing kinematics between flights, even if the bulk body motion remains similar. As found when comparing the four unaccelerating Blue Dasher flights, the pitch angles employed by

dragonflies varied significantly between specimens and on a few occasions even between subsequent wing strokes. This held true for nearly all of the kinematic parameters discussed, including stroke amplitude, wing stroke frequency, and downstroke-to-upstroke duration.

2. As a consequence of this kinematic variability, it must be warned that drawing significant conclusions from the kinematics of a single dragonfly flight, as has been done by researchers in the past [16], may lead to falsely characterizing uncommon kinematic profiles as standard. Instead, if a typical wing stroke is to be described, it must be based on kinematics found across multiple flights.

3. Although significant kinematic differences were observed between flights containing similar maneuvers, certain common factors were found as well. In the unaccelerating flights, the forewings were found to reach peak pitch angles of 35° during the downstroke and 135° during the upstroke. Thus, the wings were rotated 35° off of the stroke plane during the downstroke and 45° off of the stroke plane during the upstroke. The hindwings utilized more aggressive pitch angles, reaching values of approximately 40° during the downstroke and 115° (65° off of the stroke plane) during the upstroke.

4. A significant amount of asymmetry was found between the downstroke and upstroke durations. The downstroke was found to be shorter than the upstroke for the unaccelerating, accelerating, and climbing flights of the Blue Dasher, and for the unaccelerating flights of both the Common Pondhawk and the Spot-Winged Glider. In some cases, the downstroke represented less than

34% of the total wing stroke duration. This is directly opposed to what has been found in previous free-flying dragonfly kinematic studies [14] [15].

5. Large amounts of variability were also found in the wing stroke amplitudes. These ranged from 79 to 130° for the unaccelerating flights, but were typically held between 95 and 105°. It is theorized that since large differences in stroke amplitude were present despite the lack of noticeable maneuvers, dragonflies may use variations in their wing stroke amplitude as a tool to make small adjustments to their trim conditions.

6. The unaccelerating dragonflies utilized both moderately advanced rotation and symmetrical rotation about the stroke reversal point. This is consistent with past work which suggests that advanced and symmetric rotations both result in increased lift production during stroke reversal [30].

7. Two types of wing pitch angle profiles were observed during the translational period of the wing stroke: a plateau-type profile where the pitch angle was held fairly steady throughout the mid-stroke, and a peak-type profile where a maximum angle was held only briefly before the next wing rotation began. The plateau-type profile appeared to be most prominent in the unaccelerating dragonflies, but the peak-type (as well as combinations of the two) was common as well.

8. A unique two-step flap angle profile was observed for three separate upstrokes. Two of these occurred during unaccelerating Blue Dasher flights, and one dur-

ing the unaccelerating Spot-Winged Glider flight. The brief pause and subsequent acceleration in flap rate could be a symptom of a change in the flow structure around the wing at mid-stroke, and may be worth further investigation.

9. All twelve flights involved out-of-phase flapping between the forewings and the hindwings. In-phase flapping was never observed, suggesting that such kinematics are rarely employed. By comparison, in one study of tethered dragonflies flying in a wind tunnel, periods of in-phase flapping were observed in 48 of 91 flights [38]. Since it has been theorized that in-phase flapping is used for maximum force production, it is possible that in-phase flapping is more commonly seen in tethered flight than free-flight because the dragonflies are utilizing escape-mode kinematics.

10. Fully counterstroking (180° out of phase) flapping was not observed for any flight. Phase differences ranged from 61 to 98°, with the motion of the forewings lagging that of the hindwings for all flights.

11. The aforementioned kinematic variability between individual flights of the same type made it difficult to confidently attribute any changes in wing kinematics to variations in flight description. The only notable kinematic difference between the accelerating and unaccelerating flights was that the forewing stroke amplitudes were approximately 5° smaller for the accelerating flights. However, additional accelerating flights must be analyzed to determine if this trend is significant.

12. The primary kinematic difference observed for climbing Blue Dasher flights was that the dragonflies employed significantly more aggressive advanced rotation of the forewings than observed for the unaccelerating flights. The hindwings, however, primarily exhibited symmetrical rotation about the stroke reversal point.

13. The turning flights exhibited 15% higher wing stroke frequencies than the unaccelerating flights. Furthermore, three of the four wings were found to have longer average downstroke durations than upstroke durations. This was not found for any other types of flights. Left-right asymmetries were found in the form of larger stroke amplitudes on the inside wings, as well as a case where the dragonfly used nearly fully delayed rotation during pronation. The peak pitch angles were also found to be more aggressive than typical during the downstroke and less aggressive during the upstroke, although this was in effect for both the left and right wing pairs.

14. The Common Pondhawk in Flight 11 was found to exhibit similar wing kinematics to the Blue Dasher in unaccelerating flight. This was expected, as the two species are of approximately equal size and exhibit similar behavioral patterns in the wild. The only notable kinematic difference observed was that the Common Pondhawk tended to favor more highly advanced rotation and higher wingbeat frequencies than the Blue Dasher. However, since only two complete wing strokes were analyzed, this difference may not be statistically significant.

15. The Spot-Winged Glider was found to flap at much lower frequencies and with significantly shallower stroke amplitudes than the Blue Dasher, or any dragonfly described in Ruppell's study [14]. This is likely related to the larger size of the Spot-Winged Glider and its highly migratory nature, which emphasizes efficient flight over peak thrust production. It can be tentatively concluded that dragonflies of different sizes and flight behaviors are likely to exhibit somewhat different wing kinematics. As such, if dragonfly kinematics are being investigated as an inspiration for an MAV design, care should be taken to select a species that displays flight behavior that is best matched to the desired role of the MAV.

5.3   Considerations for Future Work

The present work represents only an initial analysis of the data recorded for hundreds of free-flying tests. Due to the time-intensive nature of the marker tracking process, it was not possible to analyze every useful flight for the purpose of this thesis. Thus, additional flights can be analyzed to more confidently establish standard wing kinematics for each type of flight. There are also many other types and sizes of locally available dragonflies that could be tested to further investigate the range of differences found in kinematics between various species.

A primary weakness of the current data is the inability to determine the roll orientation of the dragonfly with a high degree of accuracy. This prevents certain kinematic parameters (such as wing stroke plane deviation angle) from being inves-

tigated as they are directly dependent to the roll orientation of the dragonfly. Future photogrammetric investigations of dragonfly wing kinematics should ensure that an accurate method for determining the roll angle is used. For example, bright or reflective markers placed on the thorax of the dragonfly could be tracked throughout a sequence to identify the roll angle in every frame. It is also likely that spacing the video cameras further apart (assuming the absence of the physical constraints encountered in the present study) would result in more accurate body model fitting.

Of course, it must be noted that simple bio-derived flapping-wing kinematic data are not sufficient for the development of effective design tools for MAV-scale flapping-wing platforms. In order to develop a true understanding of how dragonflies utilize unsteady low Reynolds number mechanisms to fly, the flow structure around the wings must be understood through the use of tools such as computational fluid dynamics (CFD). Past CFD investigations have used greatly simplified flapping kinematics and have often neglected the effect of tandem wing pairs to focus on the performance of a single wing. The detailed flapping and pitching kinematic data presented here can serve as a realistic basis for future CFD studies and allow for more accurate modeling of the aerodynamic mechanisms responsible for keeping dragonflies aloft.

Bibliography

[1] Darryll J Pines and Felipe Bohorquez. Challenges facing future micro-air-vehicle development. *Journal of Aircraft*, 43(2):290–305, 2006.

[2] Nick T Pornsin-sirirak, Yu-Chong Tai, Chih-Ming Ho, and Matt Keennon. Microbat: A palm-sized electrically powered ornithopter. In *Proc. of NASA/JPL Workshop on Biomorphic Robotics, Pasadena, CA, 14-17 August*, pages 14–17. IEEE, 2001.

[3] Patrick Zdunich, Derek Bilyk, Marc MacMaster, and David Loewen. Development and testing of the mentor flapping-wing micro air vehicle. *Journal of Aircraft*, 44(5):1701–1711, 2007.

[4] Wei Shyy, Hikaru Aono, Chang-kwon Kang, and Hao Liu. *An introduction to flapping wing aerodynamics*, volume 37. Cambridge University Press, 2013.

[5] David Lentink and Michael H Dickinson. Rotational accelerations stabilize leading edge vortices on revolving fly wings. *Journal of Experimental Biology*, 212(16):2705–2719, 2009.

[6] Z Jane Wang and David Russell. Effect of forewing and hindwing interactions on aerodynamic forces and power in hovering dragonfly flight. *Physical Review Letters*, 99(14):148101, 2007.

[7] Yuta Ichikawa and Mamoru Watanabe. The daily food intake of pantala flavescens females from foraging swarms estimated by the faeces excreted (odonata: Libellulidae). *Odonatologica*, 44(3):375–389, 2015.

[8] RM Olberg, AH Worthington, and KR Venator. Prey pursuit and interception in dragonflies. *Journal of Comparative Physiology A*, 186(2):155–162, 2000.

[9] SA Combes, MK Salcedo, MM Pandit, and JM Iwasaki. Capture success and efficiency of dragonflies pursuing different types of prey. *Integrative and Comparative Biology*, 53(5):787–798, 2013.

[10] Matt W Hayward, Gina J Hayward, Craig J Tambling, and Graham IH Kerley. Do lions panthera leo actively select prey or do prey preferences simply reflect chance responses via evolutionary adaptations to optimal foraging? *PLoS ONE*, 6(9):1–6, 2011.

[11] AC Neville. Aspects of flight mechanics in anisopterous dragonflies. *Journal of Experimental Biology*, 37(3):631–656, 1960.

[12] Jill Silsby. *Dragonflies of the World.* Smithsonian, 2001.

[13] RJ Wootton, J Kukalová-Peck, DJS Newman, and J Muzón. Smart engineering in the mid-carboniferous: How well could palaeozoic dragonflies fly? *Science*, 282(5389):749–751, 1998.

[14] G Rüppell. Kinematic analysis of symmetrical flight manoeuvres of odonata. *Journal of Experimental Biology*, 144(1):13–42, 1989.

[15] JM Wakeling and CP Ellington. Dragonfly flight. ii. velocities, accelerations and kinematics of flapping flight. *Journal of Experimental Biology*, 200(3):557–582, 1997.

[16] Chengyu Li and Haibo Dong. Wing kinematics measurement and aerodynamics of a dragonfly in turning flight. *Bioinspiration & Biomimetics*, 12(2), 2017.

[17] CP Ellington. The aerodynamics of hovering insect flight. iii. kinematics. *Philosophical Transactions of the Royal Society of London. B, Biological Sciences*, 305(1122):41–78, 1984.

[18] Alexander P Willmott and Charles P Ellington. Measuring the angle of attack of beating insect wings: Robust three-dimensional reconstruction from two-dimensional images. *Journal of Experimental Biology*, 200(21):2693–2704, 1997.

[19] Simon M Walker, Adrian LR Thomas, and Graham K Taylor. Photogrammetric reconstruction of high-resolution surface topographies and deformable wing kinematics of tethered locusts and free-flying hoverflies. *Journal of The Royal Society Interface*, 6(33):351–366, 2009.

[20] Deqiang Song, Hao Wang, Lijiang Zeng, and Chunyong Yin. Measuring the camber deformation of a dragonfly wing using projected comb fringe. *Review of Scientific Instruments*, 72(5):2450–2454, 2001.

[21] Hao Wang, Lijiang Zeng, Hao Liu, and Chunyong Yin. Measuring wing kinematics, flight trajectory and body attitude during forward flight and turning maneuvers in dragonflies. *Journal of Experimental Biology*, 206(4):745–757, 2003.

[22] AC Carruthers, SM Walker, ALR Thomas, and GK Taylor. Aerodynamics of aerofoil sections measured on a free-flying bird. *Proceedings of the Institution of Mechanical Engineers, Part G: Journal of Aerospace Engineering*, 224(8):855–864, 2010.

[23] Christopher Koehler, Zongxian Liang, Zachary Gaston, Hui Wan, and Haibo Dong. 3d reconstruction and analysis of wing deformation in free-flying dragonflies. *The Journal of Experimental Biology*, 215(17):3018–3027, 2012.

[24] Mark A. Reavis and Marvin W. Luttges. Aerodynamic forces produced by a dragonfly. *AIAA Aerospace Sciences Meeting*, January 1988. AIAA Paper 88-0330.

[25] Chris Somps and Marvin Luttges. Dragonfly flight: novel uses of unsteady separated flows. *Science*, 228(4705):1326–1329, 1985.

[26] PS Baker, M Gewecke, and RJ Cooter. The natural flight of the migratory locust, locusta migratoria l. iii. wing-beat frequency, flight speed and attitude. *Journal of Comparative Physiology A*, 141(2):233–237, 1981.

[27] Alexander P Willmott and Charles P Ellington. The mechanics of flight in the hawkmoth manduca sexta. i. kinematics of hovering and forward flight. *The Journal of Experimental Biology*, 200(21):2705–2722, 1997.

[28] Steven Vogel. Flight in drosophila. iii. aerodynamic characteristics of fly wings and wing models. *Journal of Experimental Biology*, 46(3):431–443, 1967.

[29] CP Ellington. The aerodynamics of hovering insect flight. iv. aeorodynamic mechanisms. *Philosophical Transactions of the Royal Society of London. B, Biological Sciences*, 305(1122):79–113, 1984.

[30] Fritz-Olaf Lehmann. The mechanisms of lift enhancement in insect flight. *Naturwissenschaften*, 91(3):101–122, 2004.

[31] Diana D Chin and David Lentink. Flapping wing aerodynamics: from insects to vertebrates. *Journal of Experimental Biology*, 219(7):920–932, 2016.

[32] Michael H Dickinson and Karl G Gotz. Unsteady aerodynamic performance of model wings at low reynolds numbers. *Journal of Experimental Biology*, 174(1):45–64, 1993.

[33] Alexander P Willmott, Charles P Ellington, and Adrian L R Thomas. Flow visualization and unsteady aerodynamics in the flight of the hawkmoth, manduca sexta. *Phil. Trans. R. Soc. Lond. B*, 352(1351):303–316, 1997.

[34] James M Birch and Michael H Dickinson. Spanwise flow and the attachment of the leading-edge vortex on insect wings. *Nature*, 412(6848):729–733, 2001.

[35] Richard J Bomphrey, Toshiyuki Nakata, Per Henningsson, and Huai-Ti Lin. Flight of the dragonflies and damselflies. *Phil. Trans. R. Soc. B*, 371(1704):20150389, 2016.

[36] Darryll J Pines and Felipe Bohorquez. Challenges facing future micro-air-vehicle development. *Journal of Aircraft*, 43(2):290–305, 2006.

[37] Mao Sun and Jian Tang. Lift and power requirements of hovering flight in drosophila virilis. *Journal of Experimental Biology*, 205(16):2413–2427, 2002.

[38] David E Alexander. Unusual phase relationships between the forewings and hindwings in flying dragonflies. *Journal of Experimental Biology*, 109(1):379–383, 1984.

[39] Timothy M Broering, Yongsheng Lian, and William Henshaw. Numerical investigation of energy extraction in a tandem flapping wing configuration. *AIAA Journal*, 50(11):2295–2307, 2012.

[40] Ji Kang Wang and Mao Sun. A computational study of the aerodynamics and forewing-hindwing interaction of a model dragonfly in forward flight. *Journal of Experimental Biology*, 208(19):3785–3804, 2005.

[41] Adrian LR Thomas, Graham K Taylor, Robert B Srygley, Robert L Nudds, and Richard J Bomphrey. Dragonfly flight: free-flight and tethered flow visualizations reveal a diverse array of unsteady lift-generating mechanisms, controlled

primarily via angle of attack. *Journal of Experimental Biology*, 207(24):4299–4323, 2004.

[42] SR Jongerius and D Lentink. Structural analysis of a dragonfly wing. *Experimental Mechanics*, 50(9):1323–1334, 2010.

[43] Keith B. Atkinson. *Close Range Photogrammetry and Machine Vision*. Reinhold, 1996.

[44] R. I. Hartley and A. Zisserman. *Multiple View Geometry in Computer Vision*. Cambridge University Press, ISBN: 0521540518, second edition, 2004.